# Open Research Online

# Unveiling the X-ray point source population of the Young Massive Cluster Westerlund 1

## Journal Item

Version: Version of Record

Link(s) to article on publisher's website:
http://dx.doi.org/doi:10.1051/0004-6361:20077186

oro.open.ac.uk

**Astronomy & Astrophysics**

# Unveiling the X-ray point source population of the Young Massive Cluster Westerlund 1[*],[**]

J. S. Clark[1], M. P. Muno[2], I. Negueruela[1,3], S. M. Dougherty[4], P. A. Crowther[5], S. P. Goodwin[5], and R. de Grijs[5,6]

1. Department of Physics & Astronomy, The Open University, Walton Hall, Milton Keynes, MK7 6AA, UK
   e-mail: s.clark@open.ac.uk
2. Department of Physics and Astronomy, University of California, Los Angeles, CA 90095, USA
3. Departamento. de Física, Ingeniería de Sistemas y Teoría de la Señal, Universidad de Alicante, Apdo. 99, E03080 Alicante, Spain
4. National Research Council, Herzberg Institute of Astrophysics, Dominion Radio Astrophysical Observatory, PO Box 248, Penticton BC. V2A 6K3, Canada
5. Department of Physics & Astronomy, University of Sheffield, Sheffield, S3 7RH, UK
6. National Astronomical Observatories, Chinese Academy of Sciences, 20A Datun Road, Chaoyang District, Beijing 100012, PR China

## ABSTRACT

*Aims.* We investigate the nature of the X-ray point source population within the Young Massive Cluster Westerlund 1.

*Methods.* Chandra observations of 18 ks and 42 ks were used to determine the X-ray properties of emitters within Wd 1, while a comprehensive multiwavelength dataset was employed to constrain their nature.

*Results.* We find X-ray emission from a multitude of different stellar sources within Wd 1, including both evolved high mass and low mass pre-MS stars. We attribute the X-ray emission from the high mass component to both single stars and colliding wind binaries on the basis of their observed flux and spectral properties, with binaries being systematically harder and more luminous than single stars. We are able to infer a high binary fraction for both WN (10/16) and WC stars (7/8), resulting in a combined Wolf Rayet binary fraction of ≳70%. These represent the most stringent limits currently placed on the binary fraction of very massive (>45 $M_\odot$) stars. We place the first observational constraints on X-ray emission from stars transitioning between the Main Sequence and Wolf Rayet phases, finding that both hot (B hypergiants) and cool (yellow hypergiants and red supergiants) spectral types appear to be intrinsically X-ray faint. The B[e] star W9 is found to be X-ray bright and shows similarities to both the X-ray binary SS433 and the Luminous Blue Variable $\eta$ Carinae. Globally, we find the point source population to be systematically fainter than those found in younger massive star forming regions such as NGC 3603 and R136/30 Doradus, consistent with a loss of the most massive stars to SNe and a reduction in emissivity from the low mass pre-Main Sequence stars. No unambiguous evidence for X-ray emission due to accretion onto relativistic objects of any mass is found, although the current data do not exclude the presence of either a High Mass X-ray Binary or an Intermediate Mass Black Hole accreting at a low rate. Finally, we suggest the progenitor mass for the magnetar CXOU J164710.2-455216 is comparable to that of SGR 1806-20 (~55 $M_\odot$), while that for SGR 1900+14 appears significantly lower (~15 $M_\odot$), implying that magnetars may form from stars with a wide range of initial masses.

**Key words.** stars: evolution – open clusters and associations: individual: Westerlund 1 – X rays: stars

## 1. Introduction

Starburst galaxies are strong X-ray sources, with the emission originating in the young stellar population that results from the vigorous ongoing star formation. Characteristically, this activity yields numerous dense Young Massive Clusters (YMCs; $M_{\rm tot} \geq 10^5 M_\odot$), which one might expect to significantly contribute to the global X-ray emission of their host galaxy. However the current generation of telescopes cannot spatially resolve YMCs in external galaxies and therefore it is difficult to determine the relative contributions to their X-ray output from diffuse (cluster winds & Supernovae (SNe) remnants) and point (stellar) sources (e.g. Oskinova 2005a).

X-ray emission is associated with both high and low mass stars at many different evolutionary stages, but stellar X-ray production within YMCs is expected to be dominated by:

- T-Tauri and protostars, which demonstrate magnetic activity resulting in the production of high temperature X-ray emitting plasma, with fluxes reaching $L_X \sim 10^{31-32}$ erg s$^{-1}$ during transient flares (e.g. Feigelson & Montmerle 1999; Favata et al. 2005).
- Single OB stars emitting at $L_x \sim 10^{-7} L_{\rm bol}$ (e.g. $10^{31-33}$ erg s$^{-1}$; Long & White 1980; Seward & Chlebowski 1982) via shocks embedded in their stellar winds (e.g. Lucy & White 1980).
- Shocks between the colliding winds of OB+OB and OB+Wolf Rayet (WR) binaries ($L_x \sim 10^{32-35}$ erg s$^{-1}$; e.g. Pollock 1987).
- The post-SN relativistic remnants of >8 $M_\odot$ progenitors, via accretion in binary systems ($L_x \sim 10^{33-39}$ erg s$^{-1}$) or, more rarely, via the decay of magnetic fields (Magnetars, where

quiescent $L_x \sim 10^{33-36}$ erg s$^{-1}$; e.g. Meregheti et al. 2004) or rotational energy (radio pulsars, where $L_x \sim 10^{29-36}$ erg s$^{-1}$; e.g. Cheng et al. 2004).

By virtue of their extreme masses, the rich co-eval stellar populations of YMCs make them important laboratories for the study of such X-ray bright objects. Indeed, by identifying both low mass pre-MS stars and high mass colliding wind binaries (CWBs) X-ray observations may inform studies of the Initial Mass Function (IMF) and binary fraction of such clusters, important parameters for constraining both the formation mechanism and long term evolution of YMCs.

Moreover, it is possible that the stellar densities present in such systems may facilitate the formation of "exotic" X-ray emitting objects that are absent from less extreme star forming environments. An obvious example would be the putative "Intermediate Mass" Black Holes (IMBHs; $10^{2-4}$ $M_\odot$), which, for example, Portegies Zwart et al. (2004) propose can be produced via the runaway merger of cluster stars and which have been proposed as the central engines of Ultraluminous X-ray Sources (ULXs; $L_x \geq 10^{39}$ erg s$^{-1}$).

Consequently, significant effort has been expended determining the X-ray properties of nearby stellar clusters within which individual stellar emitters may be identified. Examples include NGC3603 (Moffat et al. 2002), and the Arches and Quintuplet clusters (Law & Yusef-Zadeh 2004; Rockefeller et al. 2005). However, each of these clusters appears to be at least an order of magnitude smaller in mass than typical YMCs, and so it is not immediately clear that they form viable templates for such objects. Recently, optical observations of the Galactic cluster Westerlund 1 (Wd 1; Clark & Negueruela 2004; Clark et al. 2005) have suggested a mass of $\sim 10^5$ $M_\odot$ and consequently that it may be the first example of a YMC in our Galaxy.

At an age of $4-5$ Myr (Crowther et al. 2006), Wd 1 is intriguingly placed at an age between stellar winds and SNe being the dominant cluster wind driver and source of X-ray emission (Oskinova 2005a). Moreover, the combination of age and large mass has resulted in a rich population of short lived transitional objects e.g. Luminous Blue Variables (LBVs), Red Supergiants (RSGs) and Yellow Hypergiants (YHGs), providing the first opportunity to quantify the X-ray properties of these stellar types, which has hitherto not been accomplished due to the rarity of such stars. Finally, we might expect $\sim 10^2$ SNe to have already occurred in Wd 1 (Sect. 7.1), providing an opportunity to study the final post-SN products of a stellar population of known age, progenitor mass and metallicity.

This manuscript is the fourth in a series of papers describing the X-ray properties of Wd 1. Previous papers have described the detection of the Anomalous X-ray Pulsar (AXP) CXO J164710.2-455216 (Muno et al. 2006a) – which Muno et al. (2007) subsequently demonstrated to be a magnetar – and the properties of the diffuse X-ray emission (Muno et al. 2006c). In this paper we complete the analysis by describing the properties of the point sources and their optical and/or near-IR counterparts. An analysis of the X-ray data by Skinner et al. (2006) associates 12 of the point sources with WR cluster members and a thirteenth with the enigmatic emission line object W9. We extend this analysis to include the global properties of the X-ray point sources, while employing new spectroscopic and photometric datasets from optical-radio wavelengths to elucidate the nature of the emitters.
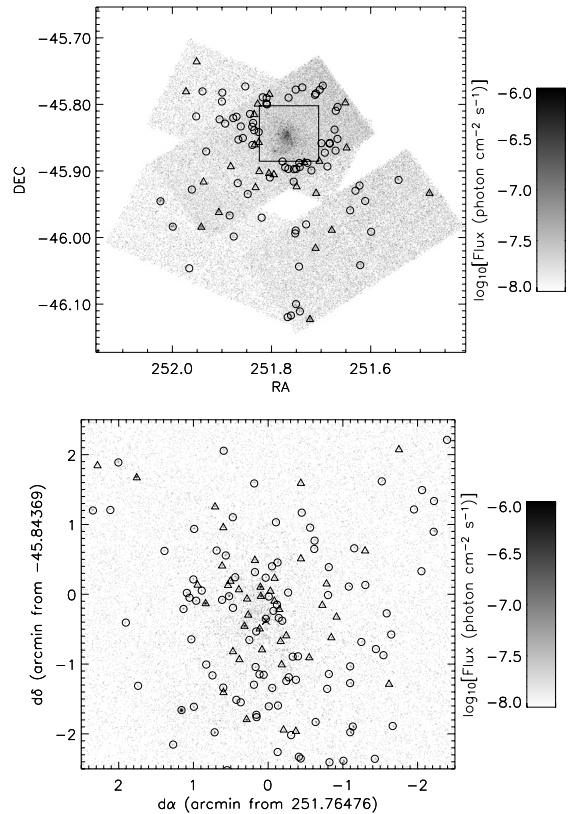


**Fig. 1.** *Top panel*: image of the locations of X-ray photons received by CCDs 0, 1, 6, and 7. The X-shaped pattern was produced because the observations were taken with different roll angles, 26° in 2005 May and 326° in 2005 June. The raw count image has been binned by a factor of 4 to enhance the contrast, and then was divided by the exposure map constructed for 2 keV photons. Point-like X-ray sources are indicated with circles and those with optical or IR counterparts by triangles (cf. Sect. 3, Tables 1 and 3). The square indicates the location of the $5' \times 5'$ field shown in the *lower panel*. For an adopted distance of 5 kpc the upper and lower panels are on a side $\sim 44$ pc and $\sim 7.3$ pc respectively.

## 2. X-ray observations

Wd 1 ($l = 339.5$, $b = -0.4$) was observed with the *Chandra X-ray Observatory* Advanced CCD Spectrometer Spectroscopic array (ACIS-S; Weisskopf et al. 2002) on 2005 May 22 for 18 ks (sequence 6283) and 2005 June 20 for 42 ks (sequence 5411). We reduced these observations using standard tools that are part of CIAO version 3.2. First, we created a composite event list for each observation. We corrected the pulse heights of the events for position-dependent charge-transfer inefficiency and excluded events that did not pass the standard ACIS grade filters and *Chandra* X-ray Center (CXC) good-time filters. We searched for intervals during which the background rate flared to $\geq 3\sigma$ above the mean level, and removed one such interval lasting 3.6 ks from sequence 5411. The composite image of the full field we analysed is displayed in Fig. 1, with a smoothed version of the central $5' \times 5'$ region displayed in Fig. 2.

We identified point-like X-ray sources in each observation using a wavelet-based algorithm, WAVDETECT (Freeman et al. 2002). For each observation, we first searched in three energy bands using a series of three images. We used the following energy bands: 0.5–8.0 keV to utilize the full calibrated energy range of the ACIS-S, 0.5–2.0 keV to improve our sensitivity to foreground X-ray sources (photons in this energy range are
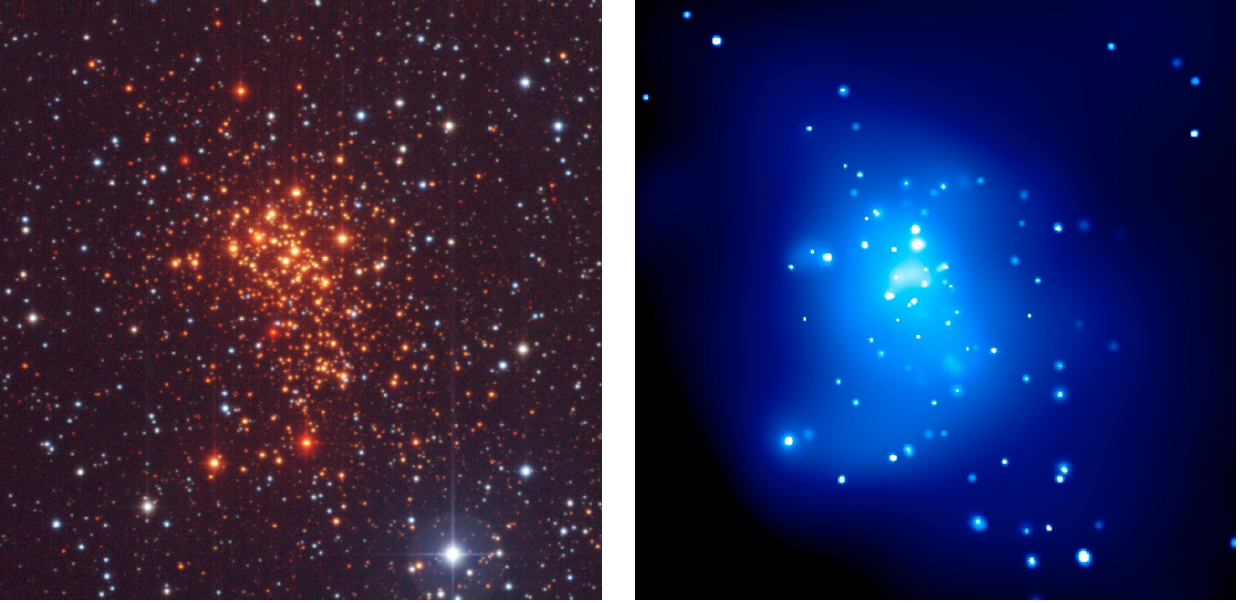
**Fig. 2.** Comparative plots of the central $5' \times 5'$ (7.3 pc on a side at 5 kpc) region of Wd 1 – *left panel*: 3 colour optical image (*V* band – blue, *R* band, green, *I* band – red), *right panel*: smoothed X-ray image from the observations presented here (an analysis of the diffuse emission is presented in Muno et al. 2006c). North is to the top and East to the right in both images.

absorbed by metals in the ISM), and 4−8 keV to provide sensitivity to highly-absorbed sources. We searched the three images for each energy band using sequences of wavelet scales that increased by a factor of $\sqrt{2}$: a central, un-binned image of 8.5′ by 8.5′ searched from scales 1−4, an image binned by a factor of two to cover 17′ by 17′ searched from scales 1−8, and an image binned by a factor of four to cover the entire field searched from scales 1−16. We used a sensitivity threshold that corresponded to a $10^{-6}$ probability of detecting a spurious source per PSF element, so that we expect only one spurious source in our search of each image (Freeman et al. 2002).

To register the astrometric frame of each observation, the locations of the point-like X-ray sources were compared to the catalogue from the Two Micron All-Sky Survey (2MASS). Based on this comparison, we were able to register the frames with an accuracy of 0.15″. In order to derive a complete list of X-ray sources, we combined the images from the two observations using the corrected astrometry, re-applied the above search algorithm, and combined the resulting source list with those derived by searching the individual observations. The complete list of candidate sources contained 241 objects. Of these there were 70 sources in the May 22 observation, 119 in the June 18 observation, and 25 in the union of the two samples. The remaining 77 faint sources were only found using the combined images.

In order to refine our estimates of the positions of each X-ray source we used the acis_extract routine from the Tools for X-ray Analysis (TARA)[1] to compute the mean position of the counts from each source, and to cross-correlate the image of each source with that of a model PSF for that location (based on the method adopted by Getman et al. 2005). For sources within 5′ of the aim point, we used the centroid of the counts received as the final position. For sources beyond 5′, we used the position derived by cross-correlating the PSF with the source photons.

We checked the positional accuracy by cross-correlating the X-ray sources with the catalogs in Sect. 3. Initially, we used

a search radius given by Eq. (5) in Hong et al. (2005), which we added in quadrature to the 0.15″ systematic uncertainty. We found that for offsets <5′ from the ACIS aim point the X-ray position of counterparts to optical/IR sources agreed to within 0.5″ in 90% of cases. We take this as our positional uncertainty for offsets <5′. It is generally an improvement over the uncertainties in the WAVDETECT positions reported by Hong et al. (2005). For larger offsets from the aim point, we found positional uncertainties consistent with Hong et al. (2005).

### 2.1. Spatial distribution

The X-ray sources in Figs. 1 and 2 appear to be highly-concentrated toward the core of Wd 1. We can estimate the number that are likely to be associated with the star cluster by comparing the number of X-ray sources in these images to the number in *Chandra* observations obtained by Ebisawa et al. (2001) of a region of the Galactic Plane at $l = 28°$ and $b = 0.2°$ that was selected to avoid known concentrations of X-ray emitting objects. Based on Monte Carlo simulations described in Muno et al. (2006a), we estimate that we can detect 90% of sources with X-ray fluxes of $6 \times 10^{-7}$ ph cm$^{-2}$ s$^{-1}$ within 5′ of the aim point in our observations of Wd 1. In the longer Galactic Plane observations of Ebisawa et al. (2001), there are 0.17 sources arcmin$^{-2}$ at this flux level. Therefore, we expect only 12 sources brighter than this completeness limit within 5′ of the aim point of our observations to be un-associated with Wd 1. Instead, we find 66 sources in the region, for an average density of 1.7 sources arcmin$^{-2}$.

Under the assumption that the excess X-ray sources are members of Wd1, we can estimate its size and centre from their distribution[2]. We assumed that the cluster profile had a Lorentzian shape (see, e.g., Nilakshi et al. 2002), and modeled the distribution by maximising the likelihood that the data would

---

[1] www.astro.psu.edu/xray/docs/TARA/

[2] Note that the density of X-ray sources is low enough such that incompleteness effects caused by crowding do not influence the result, in contrast to studies of the spatial density of optical and/or near-IR sources.
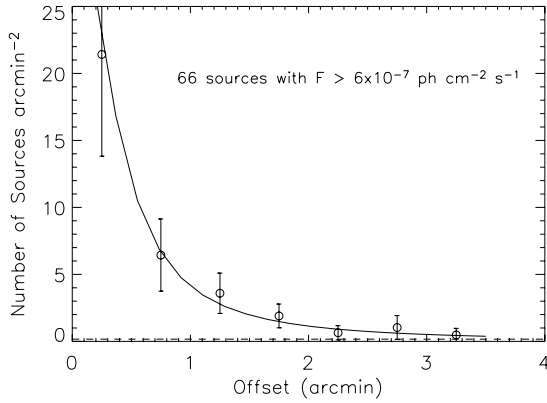
**Fig. 3.** The binned radial distribution of point sources brighter than our 90% completeness limit. We find the centroid to be at $\alpha, \delta = 16\ 47\ 03.7$, $-45\ 51\ 00$ (J2000). The solid line is the best-fit Lorentzian model of the *unbinned* distribution, which has a width of $\theta_0 = 0.3 \pm 0.1$ arcmin and a central surface density of $\rho_0 = 35^{+19}_{-13}$ sources arcmin$^{-2}$. The expected contribution from the Galactic Plane is indicated by the dashed line.

result from the assumed model. This technique is explained in Cash (1979), and was implemented by minimising

$$C = -2 \sum_i \ln P(\theta_i)$$
$$= -2 \sum_i \ln \left( \frac{1}{K} \left[ \frac{2\pi\rho_0\theta_i}{1 + \left(\frac{\theta_i}{\theta_0}\right)^2} + 2\pi\rho_c\theta_i \right] \right). \quad (1)$$

Here, $\rho_0$ is the central surface density, $\rho_c$ is a term denoting the uniform density of foreground and background sources, $\theta_0$ is the width of the spatial distribution, and

$$\theta_i = \left[ (\alpha - \alpha_0)^2 \cos^2(\delta_0) + (\delta - \delta_0)^2 \right]^{1/2} \quad (2)$$

is the offset from the assumed center of the cluster, denoted by the free parameters $\alpha_0, \delta_0$. The probability must be normalised to 1 over $\theta_i = [0, \theta_{max}]$, which is accounted for by the term $K = \pi\rho_0\theta_0^2 \ln[1 + (\theta_{max}/\theta_0)^2] + \pi\rho_c\theta_{max}^2$. We note that in order to implement this algorithm, we needed to divide the normalization $\rho_0$ out of Eq. (1), so that instead of using $\rho_c$ as a free parameter, we used the ratio $\psi = \rho_c/\rho_0$. To solve for $\rho_0$, we minimized $C$ with respect to the free parameters ($\theta_0, \alpha_0, \delta_0,$ and $\psi$), and then solved for $\rho_0$ by setting the normalization $K$ to be equal to the number of sources observed within $\theta_{max} = 5'$. The 90% uncertainties were calculated by noting that $C$ is distributed as a $\chi^2$ distribution with 1 degree of freedom. Therefore, we varied each parameter about their best-fit values, allowing the other parameters to be fit freely, until $\Delta C = 1$. We then used the upper and lower bounds of the free parameters to compute bounds on $K$, and in turn on $\rho_0$ (Lyons 1991).

The best-fit values yielded a constant background source density of $\rho_c < 0.02$ sources arcmin$^{-2}$ (a factor of 10 smaller than expected from Ebisawa et al. 2001), a full width half maximum of $\theta_0 = 0.3 \pm 0.1$ arcmin, a central density of $\rho_0 = 35^{+19}_{-13}$ sources arcmin$^{-2}$, and a centroid of $\alpha = 16^h47^m3.4^s$ ($\pm6''$), $\delta = -45°51'16''$ ($\pm12''$). The X-ray centroid is consistent with the centroid of optically-detected stars reported by Piatti et al.(1998), and the width is consistent with the 25'' core radius reported by Clark et al. (2005) and Piatti et al. (1998). Using the observed radial distribution in Fig. 3, we find that there is a significant excess of X-ray sources out to $\approx2'$ from the cluster centre. This is significantly larger than the 1.2' outer radius

reported by Piatti et al. (1998), but consistent with the angular separation of outlying cluster members as determined by Clark et al. (2005)[3]. For a distance of 5 kpc, angular radii of 0.4' and 2' correspond to 0.6 pc and 3.0 pc, respectively; we note that both high and low mass cluster members have been detected at such radii (Clark et al. in prep.; Brandner et al. 2007).

## 2.2. Photometry

We extracted photometry, spectra, and light curves for each point source using ACIS_EXTRACT, CIAO version 3.2, and HEASOFT v. 5.2. For each source, we extracted source events from within the 90% contour of the point spread function (PSF). We estimated the background contribution near the sources using annular regions around each point source that excluded $\approx92\%$ of the photons from known point sources. The outer radius of each background annulus was chosen so that it contained 100 photons. Source and background spectra were produced from the event lists, and the effective area and response functions were calculated using standard CIAO tools.

We computed the net number of counts from each source using four energy bands: 0.5–2.0 keV, 2.0–3.3 keV, 3.3–4.7 keV, and 4.7–8.0 keV. These bands were chosen so that they sampled regions of the effective area function (also known as an ancillary response function, or ARF) with roughly constant areas. The net counts in each energy band were computed from the total counts in the source region minus the estimated local background. The uncertainties on the net counts were computed by summing the squares of the 1-$\sigma$ upper limits from both the source and background counts (Gehrels 1986). We also computed 90% confidence intervals through a Bayesian analysis, with the simplifying assumption that the uncertainty on the background was negligible (Kraft et al. 1991). If the 90% confidence interval on the net counts in a band was consistent with 0, we used the 90% upper limit as the uncertainty. For 18 candidate sources, the number of net counts derived in this manner for the full band (0.5–8.0 keV) was consistent with zero, so we removed these from our catalogue. The complete catalogue of 241 X-ray sources is presented online in Table 1.

We computed approximate photon fluxes (in units of ph cm$^{-2}$ s$^{-1}$) for each source by dividing the net counts (using negative values when they occurred) in each sub-band by the total live time and the mean value of the ARF in that energy range. Note that this value incorporates variations in exposure due to chip gaps and dead columns. The sum of the photon fluxes over all of the bands (0.5–8.0 keV) are listed in Table 1, and are used throughout the paper. Since the energy bands sampled the ARF for the ACIS-I detector well, these photon fluxes differed from those derived from later spectral fits using XSPEC (Sect. 2.4) by no more than the uncertainty expected from Poisson counting noise.

## 2.3. Variability

Variability would be expected from young stellar objects, CWBs, or compact objects accreting from the winds of massive stars. To search for long-term variability, we searched for sources for which the standard deviation of the two flux measurements was larger than 3 times the uncertainty in the difference. For those sources with few counts ($\sim10$–20) identified as

---

[3] However, it should be noted that both estimates were determined from optical data alone, which would be entirely insensitive to a putative extended halo of low mass stars.

long term variables, this represents a significant detection in one observation but not the other. To search for short-term variability on the timescale of hours, we applied a Kolmogorov-Smirnov (KS) test to the un-binned arrival times of the events during each observation. If the cumulative distribution of the arrival times differed from a uniform distribution (which would imply a constant flux) with greater than 99.9% confidence in any observation, we considered the source to vary on short time-scales. In total we found that 35 out of 241 objects exhibited significant variability. In Table 1, they they are identified as either long or short term variables, as appropriate.

As described in Muno et al. (2006a), we searched for pulsars among sources with at least 50 net counts in either observation using the Rayleigh statistic ($Z_1^2$; Buccheri et al. 1983). There were 8 sources brighter than this count limit in the May observation, and 16 sources in the June observation. This lower limit on the count rate was chosen in order to detect a fully-modulated signal. The brightest source in the field, CXO J14710.2-455216, exhibited a coherent modulation with a period of 10.6 s and a root-mean-squared amplitude of 53%. None of the other sources exhibited significant signals over periods from 1.7 s to the length of the observation, with sources with between 100 and 500 net counts providing upper limits between $\approx 50$ and 25% rms.

## 2.4. Spectral analysis

In order to obtain a better understanding of the nature of the X-ray sources, we examined the spectra of the 13 sources that produced at least 80 net counts, noting that in the following analysis the data were adaptively grouped to have >20 net counts per spectral bin. The three brightest stellar sources (WR A, W30a, and W9) exhibit line emission near 1.8 and 2.5 keV (Fig. 4). These lines are near the expected energies of the He-like 2−1 transitions of Si XIII and S XV, which suggests that the X-ray emission is produced by thermal plasma. Therefore, we modeled *all* the spectra as plasma absorbed by interstellar gas and dust using the XSPEC version 11.3.1 models "phabs" and "mekal" (Arnaud et al. 1996). We assumed initially that the plasma was in collisional-ionization equilibrium (Mewe et al. 1985, 1986; Liedahl et al. 1995), and that the metals had solar abundances. This model adequately reproduced the spectra of many of the fainter sources. However, for the brighter sources, we found that residuals were present near the positions of the line emission. In three cases (W30a, the magnetar and a foreground source, CXO J164656.1 − 455314), these residuals could be removed by allowing the metal abundances to have sub-solar values.

However, in four sources (most prominently the sgB[e] W9 and the broad lined WR star, WR A) we found that the energies of the observed lines near 1.8 and 2.5 keV were $\approx 20$ eV lower than expected from Si XIII and S XV, and that the lines were unusually strong compared to the continuum. We therefore relaxed the assumption that the plasma was in collisional equilibrium (Borkowski et al. 2001), and found that the resulting model ("nei") adequately reproduced the data (following the analyis of WR140 by Pollock et al. 2005). The model parameters in the most complicated case were the column of interstellar gas and dust ($N_H$), the electron temperature of the plasma ($kT$), the metal abundance of the plasma ($Z$), the characteristic time scale for ionisation in the plasma ($n_e t$), and the normalisation of the plasma emission, which is proportional to the emission measure, $\int n_e n_H dV$. The best-fit values for all 13 sources are presented in Table 2. Seven of these sources were found to be
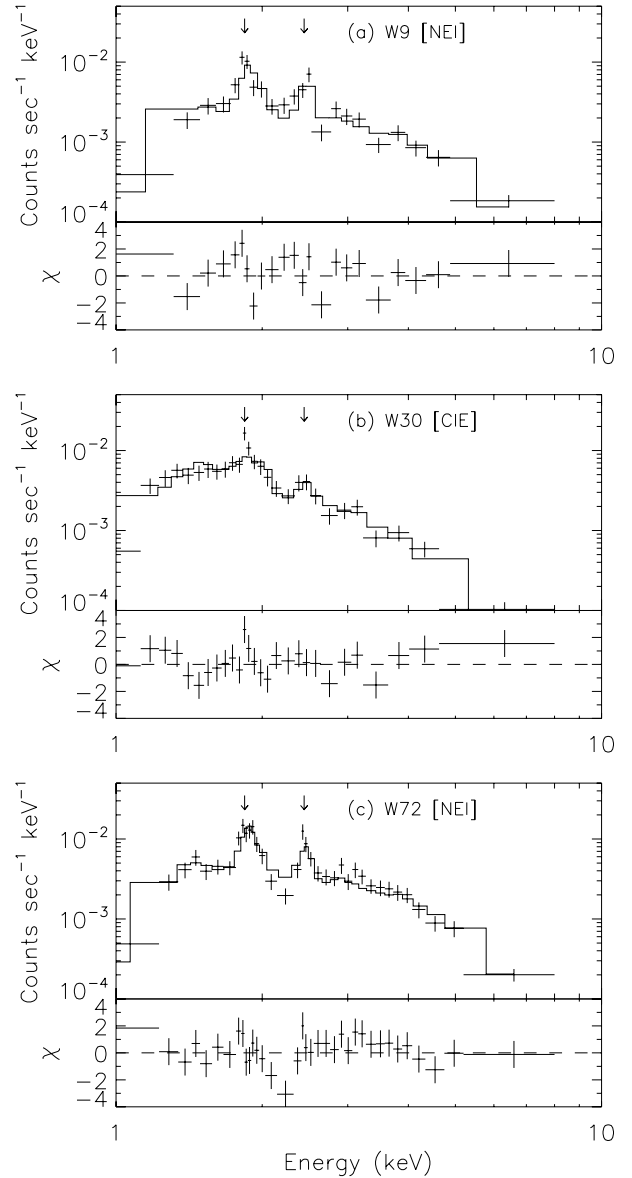


**Fig. 4.** Spectra of three of the four brightest X-ray sources (the brightest, the magnetar CXO J14710.2-455216, is displayed in Muno et al. 2006a). Note that W72 = WR A. The *top panels* display the spectra in detector counts as a function of energy, and therefore the intrinsic shapes of the source spectra are convolved with the detector response. The *bottom panels* contain the difference between the data and the best-fit plasma model, divided by the Poisson uncertainty on the data points. Prominent line emission is evident at 1.8 and 2.5 keV in each spectrum. Model parameters are listed in Table 2.

associated with massive stars within Wd 1 (Sect. 3), while of the other six, one is the magnetar, and the remaining five are likely foreground sources unconnected with Wd 1.

Our qualitative results agree with those of Skinner et al. (2006). Most of the emission is detected above 1 keV, which is not surprising given the high absorption to the cluster. The emission, with $kT \approx 2$ keV, is generally hotter than expected for isolated O/WR stars (~0.5 keV). However, the fluxes derived from our modeling are systematically lower than those derived by Skinner et al. (2006). We speculate that this is due to their model fits employing a lower temperature thermal plasma ($kT = 1$ keV) and a higher value of $N_H$ (=$3 \times 10^{22}$ cm$^{-2}$) than we find for our models, such that they assume a greater contribution from obscured, low energy emission than we do.

**Table 2.** Spectral properties of the 13 brightest X-ray point sources. Pre-empting Sect. 3, the upper panel presents those sources associated with the cluster, while the lower panel contains those sources associated with foreground objects. Source IDs are given in Col. 2, the definitions of Cols. 3−5 given in Sect. 2.4 and the normalisation is related to the emission measure by $10^{-14}/4\pi D^2 \times \int n_e n_h dV$ cm$^{-5}$. Finally, the observed and un-absorbed 0.5–8 keV fluxes are presented in Cols. 9 and 10. X-ray luminosities for individual cluster sources may be obtained by multiplying the final column by $4\pi D^2$; given the uncertain distance to the foreground sources we have refrained from presenting these.

| Source (CXO J) | Opt ID | $N_H$ ($10^{22}$ cm$^{-2}$) | $kT$ (keV) | $Z/Z_\odot$ | $\log_{10}(n_e t)$ $\log$(s cm$^{-3}$) | Norm ($10^{-4}$) | $\chi^2/\nu$ | $F_X$ $10^{-14}$ (erg cm$^{-2}$ s$^{-1}$) | $F_{uX}$ $10^{-14}$ (erg cm$^{-2}$ s$^{-1}$) |
|---|---|---|---|---|---|---|---|---|---|
| 164704.1−455107 | WR L | $1.4^{+0.4}_{-0.3}$ | $8^{+8}_{-3}$ | 1 | | $0.9^{+0.6}_{-0.2}$ | 2.9/2 | $2.4^{+0.2}_{-1.4}$ | 5 |
| 164705.3−455104 | WR B | $3.3^{+0.3}_{-0.4}$ | $1.4^{+0.3}_{-0.2}$ | 1 | $10.1^{+0.1}_{-0.3}$ | $5^{+2}_{-2}$ | 3.2/8 | $6^{+1}_{-5}$ | 730 |
| 164704.1−455039 | W30 | $1.7^{+0.1}_{-0.2}$ | $1.3^{+0.1}_{-0.1}$ | $0.3^{+0.2}_{-0.2}$ | | $6^{+1}_{-1}$ | 27.0/24 | $9.0^{+0.9}_{-2.1}$ | 52 |
| 164704.1−455031 | W9 | $2.9^{+0.2}_{-0.2}$ | $2.3^{+0.5}_{-0.3}$ | 1 | $10.8^{+0.2}_{-0.2}$ | $3.0^{+0.6}_{-0.6}$ | 37.2/19 | $10.9^{+0.9}_{-4.0}$ | 120 |
| 164706.5−455039 | WR U | $1.8^{+0.2}_{-0.3}$ | $2.8^{+1.5}_{-0.8}$ | 1 | $10.8^{+0.2}_{-0.2}$ | $0.5^{+0.2}_{-0.1}$ | 6.2/4 | $3.1^{+0.2}_{-2.5}$ | 20 |
| 164708.3−455045 | WR A | $2.6^{+0.2}_{-0.2}$ | $2.6^{+0.4}_{-0.3}$ | $0.7^{+0.2}_{-0.2}$ | $10.7^{+0.1}_{-0.1}$ | $4.5^{+1.0}_{-0.7}$ | 39.1/31 | $17^{+2}_{-4}$ | 160 |
| 164705.2−455224 | WR F | $2.3^{+0.4}_{-0.3}$ | $18^{+20}_{-6}$ | 1 | | $1.5^{+0.3}_{-0.2}$ | 2.6/3 | $4.6^{+0.8}_{-1.9}$ | 9 |
| 164710.2−455216 | AXP | $1.96^{+0.07}_{-0.11}$ | $1.5^{+0.1}_{-0.1}$ | $0.09^{+0.08}_{-0.07}$ | | $16^{+3}_{-3}$ | 55.9/48 | $24^{+2}_{-4}$ | 110 |
| 164713.6−454857 | | $0.5^{+0.1}_{-0.1}$ | $2.5^{+0.9}_{-0.5}$ | 1 | | $1.4^{+0.5}_{-0.5}$ | 1.1/3 | $1.6^{+0.2}_{-0.7}$ | 4 |
| 164720.1−455138 | | $5.1^{+1.1}_{-0.7}$ | $>10$ | 1 | | $3.1^{+0.4}_{-0.3}$ | 4.9/3 | $7.8^{+0.8}_{-2.8}$ | 18 |
| 164746.0−455904 | | $4.^{+1}_{-1}$ | $1.5^{+0.4}_{-0.3}$ | 1 | | $3^{+2}_{-1}$ | 4.7/5 | $4.8^{+1.9}_{-3}$ | 42 |
| 164656.1−455314 | | $0.32^{+0.04}_{-0.04}$ | $0.57^{+0.04}_{-0.04}$ | $0.10^{+0.04}_{-0.02}$ | − | $3.5^{+0.8}_{-0.8}$ | 31.7/22 | $4.9^{+0.7}_{-2.3}$ | 16 |
| 164653.3−460722 | | $0.13^{+1.5}_{-0.9}$ | $4^{+3}_{-1}$ | 1 | | $1.0^{+0.7}_{-0.3}$ | 2.1/4 | $3.1^{+0.6}_{-1.7}$ | 4 |

We note that when fitting the spectrum of the magnetar with a thermal plasma, the lack of line emission (low inferred metal abundances) makes it distinctly different from the stellar sources. The spectrum is best described by an optically thick blackbody (Muno et al. 2006a). This suggests that in X-ray observations of other star clusters, pulsars can be selected by searching for sources that lack X-ray line emission and have no optical/IR counterparts.

Finally, we computed an X-ray colour for *all* sources, defined as the fractional difference between the count rates in two energy bands, $(h-s)/(h+s)$, where $s$ is the number of counts in the 0.5−2.0 keV energy band, and $h$ is the number of counts in the 2.0−8.0 keV band. The resulting ratio is bounded by −1 and +1. The hardness ratios are listed in Tables 1 and 3, with uncertainties calculated according to Eq. (1.31) in Lyons (1991; p. 26). In Fig. 5, we display the photon flux and hardness of each source. Using the Portable Multi-Mission Simulator (PIMMS)[4] and XSPEC, we simulated the colours and fluxes produced by a thermal plasma spectrum absorbed by a column equivalent to $2 \times 10^{22}$ cm$^{-2}$ of H (appropiate for the extinction to the cluster), for a range of temperatures and intrinsic luminosities (0.5−8.0 keV, assuming $D = 5$ kpc). The resulting grid is over-plotted in Fig. 5.

## 3. Multiwavelength correlation and spectral classification

We have employed data from a number of other surveys to constrain the multiwavelength properties of the X-ray point source population of Wd 1. Optical data used here includes the material published in Clark et al. (2005) and Negueruela & Clark (2005). Additional $R$ and $I$ band spectroscopy was obtained on 2004 June 11−13 with FORS2 mounted on the VLT/UT1 and on 2006 February 15−17 with EMMI on the NTT (Negueruela et al., in prep.). JHKs broadband photometric observations of a $4.5' \times 4.5'$ field centred on Wd 1 were obtained with NTT/SofI on 2001 June 9 (Brandner et al. 2007). Additional near-IR narrow band imaging observations designed to identify cluster WRs

were made on 2004 May 1, with follow up IJ and HK classification spectroscopy on 2005 June 29−30 (Crowther et al. 2006)[5].

### 3.1. Optical and near-IR cross correlation

To determine the optical/near-IR counterparts of the X-ray sources associated with Wd 1 we have relied primarily on the deepest optical and near-IR photometric datasets available to us which cover a significant proportion of the cluster (Clark et al. 2005; Brandner et al. 2007). Fortuitously, both are complementary to one another. The optical data are sensitive down to $V \sim 20$ mag, which we expect to correspond to ∼O7-8V stars (∼35 $M_\odot$; Crowther 2003) and the near-IR data saturates for objects brighter than $Ks \sim 9−10$, with ∼O7-8V stars expected to have magnitudes $Ks \sim 10−11$. Thus the optical data are expected to sample the massive evolved component of Wd 1, while the near IR data sample the Main Sequence, potentially down to ∼solar mass stars[6]

The advantage of this approach is that we are utilising well-defined datasets for which the effects of, for example, incompleteness as a result of the crowding in the near-IR data, are well understood. Moreover, the multiwavelength nature of the data, when combined with the spectroscopic information available for a large number of stars, makes both the discrimination of cluster members and their subsequent spectral classification possible. However, the clear disadvantage is that we are limited to the relatively small fields surveyed (e.g. ∼$4.5' \times 4.5'$ for the SofI field). With a total of 113 X-ray sources within this region, a number of bona fide cluster sources are likely to excluded from this analysis (cf. Sect. 2.1)

---

[5] HST NICMOS data were also obtained for selected fields within the NTT/SofI fields, but the only counterparts to X-ray sources identified already had optical counterparts (Sect. 3.1) and hence these observations are not described further.

[6] The effects of incompleteness due to crowding dominate the detection threshold for faint near-IR sources. As described in Brandner et al. (2007) this results in a significantly reduced sensitivity for the crowded inner regions of the cluster, which also host the majority of the X-ray point sources. Consequently, we conservatively choose to employ the 50% completeness limit of $Ks = 16$ mag. found for the core region as the detection threshold for the NTT/SofI dataset.

---

[4] http://heasarch.gsfc.nasa.gov/Tools/w3pimms.html

**Table 3.** Summary of the X-ray and optical properties of the X-ray point sources with high mass stellar counterparts. Columns 1−3 summarise the X-ray nomenclature, photon counts and Hardness Ratio, noting that only 164706.2-455048 was found to be variable in these observations; we highlight this by presenting the photon count in italics. Column 4 is the number of the source on the finding chart (Fig. 6); we *strongly* advise that these numbers should not form the basis for a new naming convention. Column 5 contains the optical designation (sources with 2MASS or Piatti et al. (1998) designations are indicated), with Cols. 6−9 presenting relevant broadband *BVRI* photometry. The current spectral classifications for the counterparts are given in Col. 10, noting that for those sources for which no entry is given but for which photometric data are available, we predict a spectral classification earlier than B0.5Ia (Sect. A.3). Finally, in Col. 11 we flag those stars which Bonanos (2007) find to be **E**clipsing, **P**eriodic or **A**periodic photometric variables.

| X-ray Identifier | Counts | HR | Finder | Opt. ID | B | V | R | I | Spec Type | Var.? |
|---|---|---|---|---|---|---|---|---|---|---|
| 164703.7-455058 | $27.2^{+6.1}_{-5.8}$ | $-0.15^{+0.21}_{-0.21}$ | 1 | C07-X1 | 20.4 | 18.35 | 16.18 | 13.66 | | |
| 164704.1-455107 | $80.8^{+9.6}_{-10.3}$ | $0.34^{+0.11}_{-0.11}$ | 2 | WR L | 22.6 | 18.86 | 15.61 | 12.52 | WN9h: | A |
| 164702.7-455057 | $14.1^{+4.6}_{-4.0}$ | $-0.21^{+0.30}_{-0.31}$ | 3 | W41 | 21.3 | 17.87 | 15.39 | 12.78 | O9-9.5Ia | |
| 164704.4-455109 | $13.9^{+3.8}_{-4.8}$ | $0.02^{+0.31}_{-0.31}$ | 4 | – | – | – | – | – | | |
| 164702.6-455050 | $35.6^{+6.1}_{-6.5}$ | $-0.24^{+0.17}_{-0.17}$ | 5 | W40a | 22.2 | 18.05 | 15.38 | 12.73 | OB SG | |
| 164705.0-455055 | $43.4^{+7.2}_{-7.4}$ | $-0.79^{+0.13}_{-0.11}$ | 6 | W36 | 22.8 | 18.89 | 16.09 | 13.38 | | E |
| 164702.8-455046 | $9.0^{+4.2}_{-3.6}$ | $-0.39^{+0.41}_{-0.43}$ | 7 | W38 | 23.2 | 19.10 | 16.47 | 13.81 | | |
| 164705.3-455104 | $237.5^{+16.1}_{-16.5}$ | $0.21^{+0.06}_{-0.07}$ | 8 | WR B | – | 20.99 | 17.50 | 14.37 | WN7o | E |
| 164703.0-455043 | $10.9^{+3.7}_{-4.9}$ | $-1.00^{+0.55}$ | 9 | – | – | – | – | – | | |
| 164702.1-455112 | $19.3^{+5.4}_{-5.2}$ | $0.14^{+0.27}_{-0.27}$ | 10 | W24 | 23.0 | 18.71 | 15.96 | 13.24 | O9-9.5Ia | |
| 164703.4-455039 | $5.9^{+3.2}_{-4.3}$ | $1.00_{-1.03}$ | 11 | C07-X2 | 23.1 | 19.55 | 16.71 | 13.95 | | |
| 164704.1-455039 | $552.2^{+24.9}_{-24.5}$ | $-0.15^{+0.04}_{-0.04}$ | 12 | W30a | 22.4 | 18.45 | 15.80 | 13.20 | O9-B0.5Ia bin | |
| 164702.5-455117 | $18.0^{+4.8}_{-6.0}$ | $0.22^{+0.30}_{-0.29}$ | 13 | W47 | 22.7 | 19.95 | 16.36 | 13.68 | | |
| 164705.1-455041 | $32.9^{+5.8}_{-6.9}$ | $-0.72^{+0.15}_{-0.14}$ | 14 | W27 | 21.5 | 17.94 | 15.35 | 12.80 | OB SG | |
| 164704.0-455124 | $19.2^{+5.5}_{-5.1}$ | $0.55^{+0.25}_{-0.25}$ | 15 | WR G | – | 20.87 | 17.75 | 14.68 | WN7o | A |
| 164703.3-455034 | $10.2^{+3.8}_{-3.5}$ | $-0.43^{+0.34}_{-0.32}$ | 16 | W10 | – | – | – | – | O9-B0.5Ia SB2 | A |
| 164706.2-455048 | $7.2^{+4.0}_{-3.8}$ | $-1.00^{+0.63}$ | 17 | W17 | 22.7 | 18.87 | 16.19 | 13.56 | | |
| 164704.1-455031 | $462.2^{+22.7}_{-22.4}$ | $0.23^{+0.05}_{-0.05}$ | 18 | W9 | 21.8 | 17.47 | 14.47 | 11.74 | sgB[e] | A |
| 164705.7-455033 | $11.2^{+4.0}_{-3.6}$ | $-1.00^{+0.36}$ | 19 | W25 | 21.9 | 17.85 | 15.22 | 12.61 | OB SG | A |
| 164706.5-455039 | $161.2^{+13.6}_{-13.2}$ | $-0.14^{+0.08}_{-0.08}$ | 20 | WR U | 23.7 | 19.81 | 16.98 | 13.99 | WN6o | |
| 164703.0-455023 | $11.1^{+3.9}_{-3.3}$ | $-0.47^{+0.31}_{-0.29}$ | 21 | W6 | 22.2 | 18.41 | 15.80 | 13.16 | O9-B0.5Ia bin | P |
| 164706.2-455126 | $14.3^{+4.7}_{-4.6}$ | $1.00_{-0.19}$ | 22 | WR D | – | – | – | – | WN7o | A |
| 164705.7-455133 | $12.7^{+3.6}_{-4.2}$ | $-0.08^{+0.31}_{-0.31}$ | 23 | 2MASS | – | – | – | – | | E |
| 164702.5-455137 | $15.3^{+4.5}_{-4.3}$ | $-0.51^{+0.27}_{-0.26}$ | 24 | W62a | – | – | – | – | O9-9.5Iab | A |
| 164706.6-455029 | $10.2^{+3.7}_{-3.3}$ | $-0.62^{+0.30}_{-0.28}$ | 25 | W15 | 22.8 | 18.96 | 16.38 | 13.75 | O9-9.5Ia | A |
| 164706.4-455026 | $18.9^{+4.1}_{-5.2}$ | $0.14^{+0.24}_{-0.24}$ | 26 | W13 | 21.1 | 17.19 | 14.63 | 12.06 | BIa$^+$ | E |
| 164706.0-455022 | $30.8^{+5.9}_{-6.8}$ | $0.27^{+0.20}_{-0.20}$ | 27 | WR R | – | – | – | – | WN5o | A |
| 164703.8-455146 | $12.6^{+3.5}_{-4.0}$ | $0.47^{+0.26}_{-0.28}$ | 28 | W65 | 22.9 | 18.73 | 16.27 | 13.68 | | |
| 164659.3-455046 | $11.3^{+3.6}_{-3.6}$ | $-0.27^{+0.32}_{-0.31}$ | 29 | W1 | 21.9 | 18.37 | 16.09 | 13.65 | | |
| 164700.3-455131 | $56.7^{+7.6}_{-8.2}$ | $-0.58^{+0.12}_{-0.11}$ | 30 | W53 | 22.9 | 18.51 | 15.80 | 13.13 | | P |
| 164708.3-455045 | $743.7^{+27.3}_{-27.3}$ | $0.19^{+0.04}_{-0.04}$ | 31 | WR A | – | 19.69 | 16.59 | 13.68 | WN7b | P |
| 164704.5-455008 | $14.2^{+4.2}_{-3.9}$ | $-0.42^{+0.27}_{-0.25}$ | 32 | C07-X3 | 21.9 | 18.89 | 16.37 | 13.76 | O9-9.5Ia | A |
| 164658.6-455114 | $15.3^{+4.3}_{-4.1}$ | $-0.07^{+0.27}_{-0.27}$ | 33 | p83 | – | – | – | – | | |
| 164701.4-455150 | $9.9^{+3.0}_{-4.0}$ | $-0.43^{+0.34}_{-0.33}$ | 34 | W59 | 23.1 | 18.97 | 16.33 | 13.64 | | |
| 16468.2-455056 | $12.7^{+3.5}_{-4.1}$ | $-0.18^{+0.30}_{-0.29}$ | 35 | 2MASS | – | – | – | – | | |
| 164659.0-455028 | $10.4^{+3.4}_{-3.5}$ | $-1.00^{+0.30}$ | 36 | W84? | 21.3 | 17.82 | 15.60 | 13.63 | | |
| 164707.0-455012 | $9.3^{+3.4}_{-3.2}$ | $-0.75^{+0.29}_{-0.24}$ | 37 | W74 | – | – | – | – | O9-9.5Ia | A |
| 164701.0-455006 | $14.5^{+3.9}_{-4.1}$ | $-0.43^{+0.26}_{-0.25}$ | 38 | – | – | – | – | – | | |
| 164708.9-455029 | $8.7^{+3.2}_{-3.8}$ | $-0.09^{+0.40}_{-0.42}$ | 39 | 2MASS | – | – | – | – | | |
| 164658.8-455145 | $14.5^{+3.9}_{-4.2}$ | $-0.02^{+0.28}_{-0.28}$ | 40 | W56b | 22.8 | 18.88 | 16.36 | 13.76 | | |
| 164707.8-455147 | $14.5^{+3.9}_{-4.2}$ | $0.40^{+0.25}_{-0.27}$ | 41 | – | – | – | – | – | | A |
| 164705.9-455208 | $8.0^{+4.0}_{-3.3}$ | $-0.57^{+0.39}_{-0.40}$ | 42 | WR E | – | – | – | – | WC9 | A |
| 164702.7-455212 | $12.3^{+3.8}_{-3.7}$ | $-0.02^{+0.30}_{-0.30}$ | 43 | C07-X4 | 23.5 | 19.29 | 16.69 | 14.09 | O9-9.5Iab | |
| 164705.2-455224 | $109.6^{+10.9}_{-11.3}$ | $0.63^{+0.08}_{-0.08}$ | 44 | WR F | 21.7 | 17.86 | 15.39 | 12.90 | WC9d | A |
| 164706.9-454940 | $12.6^{+3.6}_{-4.0}$ | $-0.33^{+0.29}_{-0.28}$ | – | – | – | – | – | – | | A |
| 164702.3-455233 | $9.9^{+2.8}_{-3.8}$ | $-0.54^{+0.31}_{-0.28}$ | 45 | C07-X5 | 22.6 | 18.96 | 16.43 | 13.81 | | |
| 164701.4-455235 | $11.9^{+3.1}_{-4.2}$ | $-0.25^{+0.30}_{-0.29}$ | 46 | C07-X6 | 21.3 | 17.53 | 15.25 | 12.85 | | A |
| 164711.5-455000 | $5.1^{+3.1}_{-2.5}$ | $1.00_{-0.49}$ | – | – | – | – | – | – | | |
| 164707.6-455235 | $54.5^{+7.7}_{-8.1}$ | $0.07^{+0.14}_{-0.14}$ | – | WR O | – | – | – | – | WN6o | A |
| 164707.6-454922 | $21.1^{+5.2}_{-4.8}$ | $0.72^{+0.16}_{-0.19}$ | 47 | WR W | – | – | – | – | WN6h | |
| 164654.2-455154 | $9.7^{+3.0}_{-3.6}$ | $-0.54^{+0.32}_{-0.29}$ | – | C07-X7 | 23.6 | 18.93 | 16.08 | 13.26 | | |
| 164707.8-455147 | $14.5^{+3.9}_{-4.2}$ | $0.40^{+0.25}_{-0.27}$ | – | – | – | – | – | – | | |
| 164659.8-455525 | $11.3^{+3.7}_{-3.6}$ | $0.57^{+0.25}_{-0.29}$ | – | WR N | – | – | 16.9 | 13.0 | WC9d | |
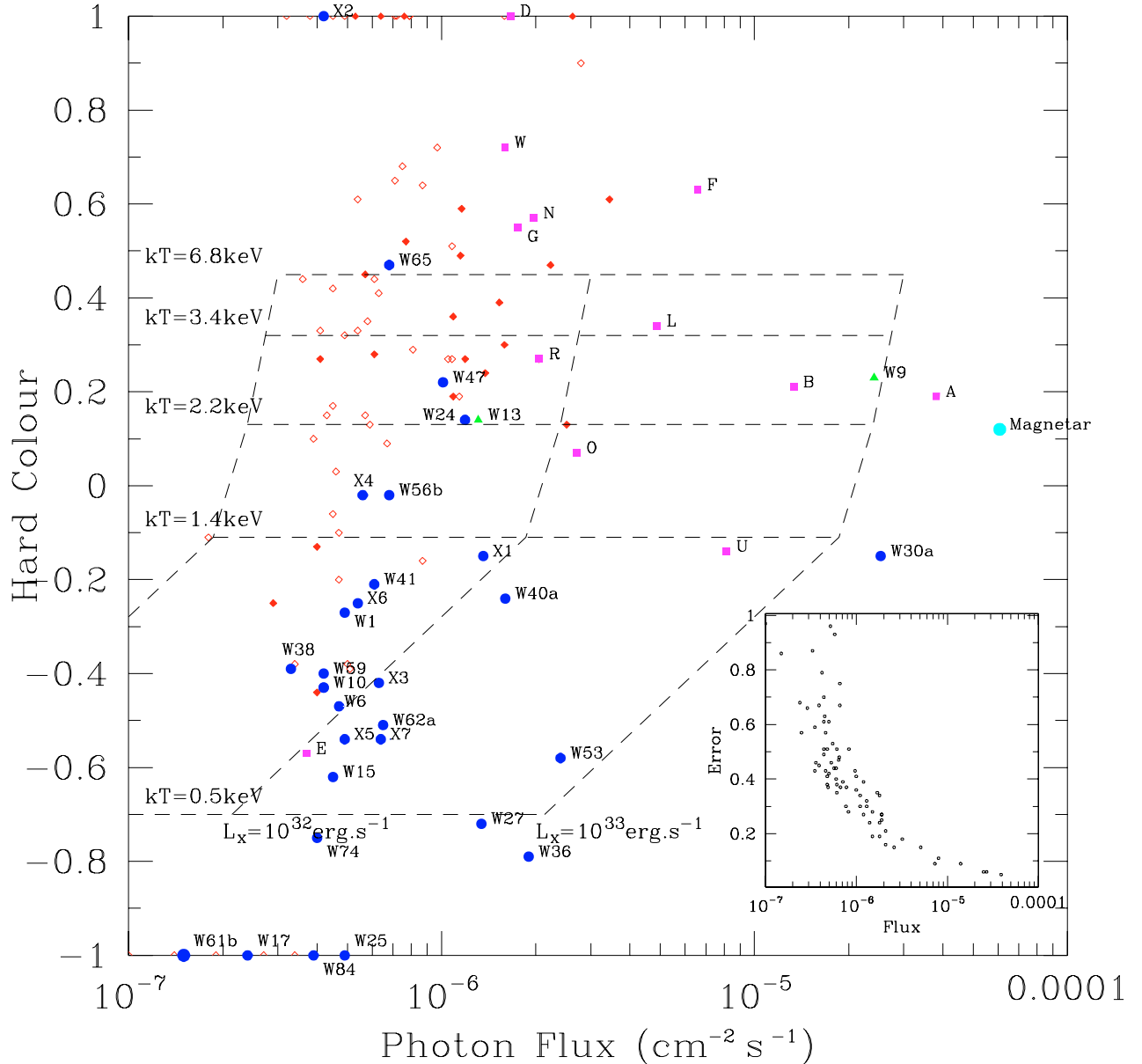
**Fig. 5.** Hardness-intensity diagram illustrating the spectral properties as a function of intensity for the X-ray point sources within the $5' \times 5'$ field centred on Wd 1. The colours are defined as $(h - s)/(h + s)$ where $h$ are the counts in the 2.0−8.0 keV band and $s$ are the counts in the 0.5−2.0 keV band. Errorbars are not shown for reasons of clarity but are inversely correlated to flux and are given for individual sources in Tables 1 and 3; the error in the hardness colour as a function of photon flux is also shown in the subpanel. Symbols are coded on the basis of their optical/near-IR counterparts: violet squares – WRs, green triangles – transitional stars, blue circles – OB supergiants and red diamonds – sources without counterparts (assumed to low mass pre-MS stars). For this final subset of sources the (empty) filled symbols represent (non) variable emission. The grid of dashed lines illustrate the fluxes and colours expected for a thermal plasma with the temperatures and luminosities indicated, absorbed by $N_H = 2 \times 10^{22}$ cm$^{-2}$ at an assumed distance of 5 kpc.

Since the stellar source list derived from Clark et al. (2005) is known to be incomplete due to the effects of blending, stars falling in the gap between the twin CCDs, and the detection of faint stars in only a subset of wavebands, we supplemented the stellar source list with the photometric datasets of Piatti et al. (1998), the USNO-B1.0 survey (Monet et al. 2003) and the 2MASS catalogue (Cutri et al. 2003; noting that our near-IR dataset is significantly deeper). Finally, we also included those stars for which no photometric data were available, but spectroscopic data suggested were bona fide cluster members such as the optically faint WR population.

Initially, we attempted an automated cross correlation between the positions of all the X-ray sources given in Table 1 and our combined stellar source list, employing a search radius of 0.5″[7]. Where available, photometric data were used to exclude foreground objects, notably four stars with USNO-B1.0 $B$-band detections. Subsequently, we relaxed the search radius

---

[7] For completeness, a cross correlation between the 2MASS and USNO-B1.0 datasets and the entire X-ray field was performed, utilising a search radius of 0.5″ within 5′ of the aim point, and 1″ beyond that offset. The results are presented in Table 1, but are not discussed further.
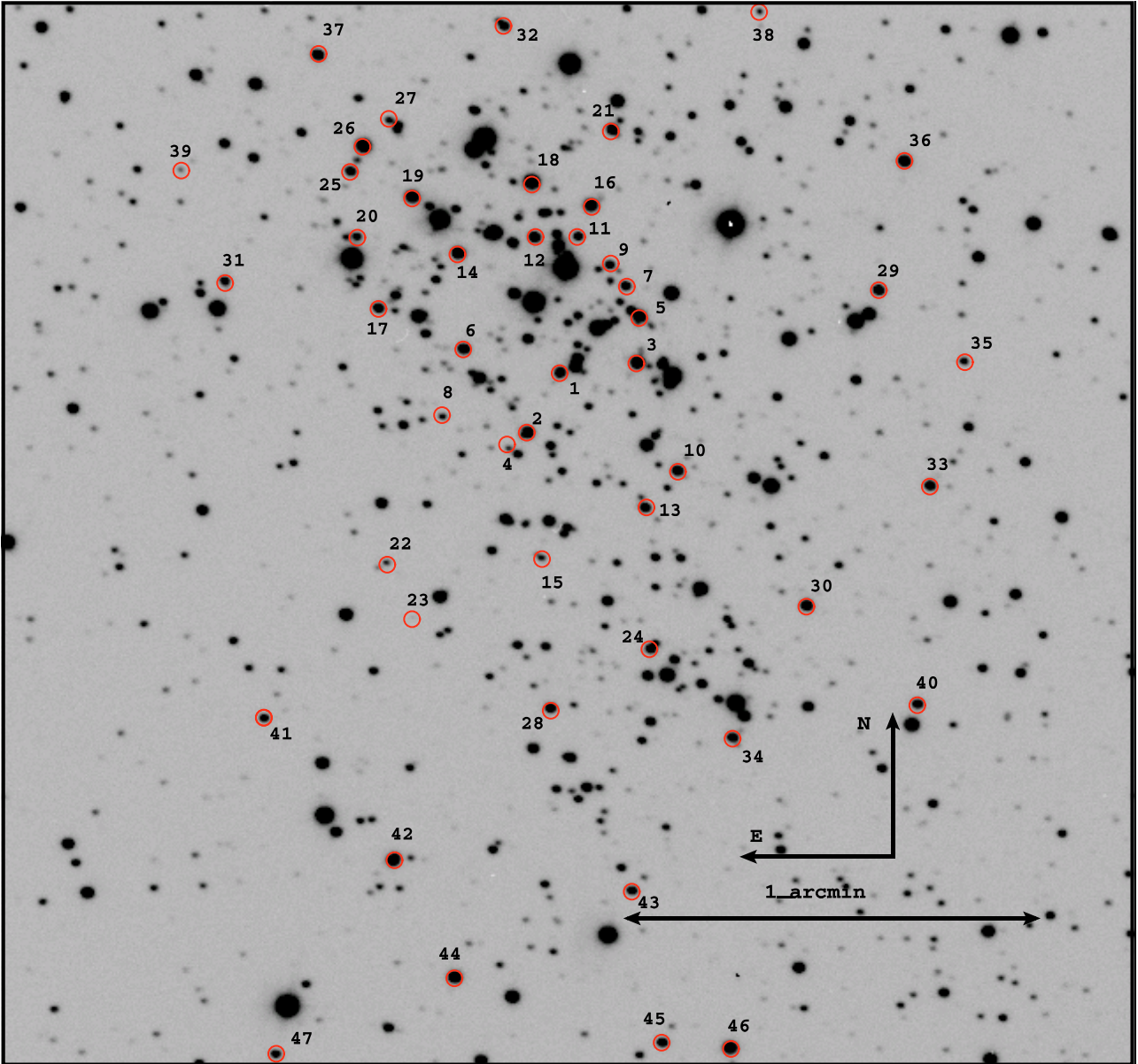
**Fig. 6.** Finding chart for the X-ray sources with optical counterparts in the crowded inner region of Wd 1. The image is in the *R* Band and taken with VLT/FORS1 in ∼0.6″ seeing conditions. Note that the size of the circles does not correspond to the positional uncertaity of the X-ray sources and is merely illustrative.

to 1″ and again utilised photometry to exclude interlopers, yielding an additional 6 potential candidates. The complete source list was then examined by eye in the deep *R*-band image presented in Fig. 6 to check for possible source confusion. A final total of 53 candidate cluster members are found to be associated with X-ray point sources, given in Table 3. We note that by randomly shifting the locations of the X-ray sources, we established with 90% confidence that at most four of these matches are spurious.

Of the final counterpart list, seven stars with X-ray emission lack both spectroscopic and photometric confirmation of cluster membership (the latter due to blending). These have been retained in order to exclude them from consideration as potential low mass stars (see below), but are not considered further in any subsequent analysis. An additional four stars were identified as cluster candidates via 2MASS or Piatti et al. (1998) colours and magnitudes. These are identified in Table 3. X-ray emission

was also associated with seven hitherto anonymous cluster members for which additional data are available. We have designated these as C07-X1 through C07-X7 in Table 3. Finally, where possible, we utilised our combined spectroscopic and photometric datasets to provide spectral classifications for the optical counterparts to the X-ray sources. This procedure is described in detail in Appendix A and the results presented in Table 3.

After this analysis, 60 X-ray point sources are left lacking optical, and hence high mass post-Main Sequence, counterparts. We might expect 5 of these to be interlopers based on the results of Ebisawa et al. (2001; Sect. 2.1). In order to determine the nature of these 60 sources, an identical cross correlation with the near-IR dataset (Brandner et al. 2007) was performed. We find that only 10 of these X-ray sources are within 0.5 arcsec of an IR source. Monte Carlo simulations of randomly positioned

X-ray sources *or* IR sources find that chance associations between the sources account for an average of 3.3 of these associations[8]. Therefore, we conclude that only ~7 of the 60 X-ray sources are associated with an IR source and that there is *no* statistically significant association between the vast majority of X-ray sources that lack optical counterparts and the IR sources. Thus we may associate the X-ray sources with no IR counterpart with a (stellar) population with apparent $K$s band magnitudes $\geq 16$. All we may conclude regarding the ~7 sources with IR counterparts is that they have $K$s magnitudes in the range ~9−16.

### 3.2. Photometric variables

Of the 53 X-ray bright high mass cluster members, 24 are identified by Bonanos et al. (2007) as variable (Table 3). These are broken down into 4 eclipsing systems, 3 periodic and 17 aperiodic variables. Based on the results presented in Appendix A, of the 4 eclipsing systems we may refine the classification of W13 to early B hypergiant and photometrically classify W17 as earlier than B0 Ia. While periodic variability might be attributed to stellar pulsations, of the 3 systems exhibiting this behaviour Crowther et al. (2006) identify the spectroscopic signature of an OB companion to WR A, while the optical spectrum of W6 is also suggestive of a short period interacting binary (Appendix A), as are the X-ray properties of W53 (Sect. 4.3). Therefore, we prefer an explananation of either ellipsiodal modulation and or wind perturbation via binary interaction for the variability in these sytems. The remaining aperiodic variables comprise WRs, OB SGs and the sgB[e] star W9; it appears likely that more than one physical mechanism causes the variability.

## 4. The high mass stellar sources

The *Chandra* X-ray observations of Wd 1 reveal a rich population of X-ray point sources of assumed stellar origin. Given that at an age of ~4−5 Myr a number of physical mechanisms could lead to this emission, we have coded the flux/hardness ratio plot for sources within the central $5' \times 5'$ field (Fig. 5) with the spectral classification of their optical counterparts in order to determine the nature of the emission. Furthermore, we identify those sources for which no optical or IR counterparts are found, delineating the subset of these that show variability. Note that only one source with an optical counterpart is found to be variable – the O SG binary W17 (Sect. 4.3).

Sources are segregated in Fig. 5 on the basis of the optical counterparts, or lack thereof. With the exception of the faint, variable source associated with WR E, the WR stars are associated with hard (hardness colour $\gtrsim -0.1$), relatively bright sources (photon flux $\gtrsim 10^{-6}$ cm$^{-2}$ s$^{-1}$). The two transitional stars detected also have similar X-ray properties. The OB SGs appear to be significantly softer and/or fainter, with the notable exception of W30a (see Sect. 4.3). We assume that those sources lacking counterparts are low mass ($<1.5$ $M_\odot$; Sect. 5) pre-MS stars (Sect. 5). The majority of these are found to be uniformly faint (photon flux $\lesssim 10^{-6}$ cm$^{-2}$ s$^{-1}$) and hard (hardness colour $\gtrsim -0.3$). A subset of OB SGs and WRs are found within the periphery of this region. It is unclear if the emission from these object is intrinsic to the massive star or is the result of an unseen low mass companion.

Globally, we find the X-ray point sources within Wd 1 to be systematically fainter than those of the massive cluster NGC 3603 (Moffat et al. 2002) and the Carina (Albacete Colombo et al. 2003) and 30 Doradus (Townsley et al. 2006a) star forming regions. While all four regions host early-type stars with a wide range of intrinsic X-ray luminosities (~two orders of magnitude), Wd 1 lacks stellar sources with luminosities significantly in excess of $10^{33}$ erg s$^{-1}$, while the other three younger stellar systems all contain sources of between $10^{34}$−$10^{35}$ erg s$^{-1}$. This finding is consistent with the prediction of Oskinova (2005a) for a rapidly diminishing contribution from stellar point sources with age as the high mass objects with powerful winds are lost to SNe, and the emission from low mass stars decreases with magnetic activity (Sect. 5).

### 4.1. The Wolf Rayets

We find 12 of the 24 WR stars within Wd 1 to be X-ray sources, while Skinner et al. (2006) associate emission with 13. There are 11 sources in common between the two studies. Skinner et al. include W9 within their sample, which we formally classify as a sgB[e] star (albeit a likely binary Sect. 4.2.1), while we find the association of X-ray emission to be in error for the WC star WR K[9]. We identify emission from the newly discovered WN6o star WR U[10], which is a bright, non variable source with a hard spectrum ($kT$ = 2.6 keV; Table 2).

We find that the distribution of the spectral subtypes of X-ray bright WRs is formally consistent with being drawn from the parent population, although we highlight that neither of the two WN8 stars were detected with the WAVDETECT algorithm employed for source selection (Sect. 2), mirroring previous non detections of such stars in X-rays (Oskinova 2005a). To the best of our knowledge WRs F and N represent the first X-ray detections of WC9d stars.

Based on the high temperatures implied by the spectral fits, Skinner et al. (2006) propose that a significant number of the WN stars are likely to be (colliding-wind) binaries. Moreover, Oskinova et al. (2003) demonstrate that no single WC star is known to be an X-ray source. Thus the X-ray detections of WR E, F and N indicate that they are likely binaries. The presence of hot dust, resulting in excess IR emission, is thought to be another indicator of binarity for WC stars, with Williams et al. (2005) proposing that the high densities that characterise the wind-interaction regions of CWBs are required for dust condensation. Analysis of the spectral energy distributions of the WCs (Crowther et al. 2006) shows that with the exceptions of WR E and K, all have excess near to mid-IR emission and are therefore strong binary candidates even in the absence of X-ray emission from all but WR N & F. Finally, the ~flat ($\alpha \sim 0$ for $S_\nu \propto \nu^{-\alpha}$) radio spectra of WR A, B and V imply contributions from both thermal+non thermal emission mechanisms as expected for CWB systems (Dougherty et al. 2007). Such a result is of particular interest for WR V as to date it shows no other indication of binarity.

Including the WN10-11h/BIa$^+$ star WR S, of the 16 WN stars, 9 are observed to be hard X-ray sources, while WR V demonstrates a composite radio spectrum. This implies a binary fraction of $\gtrsim 63\%$ for WN stars although only

---

[8] We note that randomly distributing either the X-ray or IR sources does not account for the obvious clustering in both, however including this clustering would *increase* the number of chance associations.

[9] The position of the X-ray source attributed by Skinner et al. (2006) is found to be ~2.3″ to the West of the position of WR K in Crowther et al. (2006).

[10] Note that WRs #1 & #3 of Groh et al. (2006) are our WR U & W respectively.

**Table 4.** Limits on the count rates from spectroscopically-identified stars. Limits on the luminosities can be derived by noting that 1 count is equivalent to $2 \times 10^{30}$ erg s$^{-1}$ for a 3 keV plasma at $D = 5$ kpc, and $1 \times 10^{31}$ erg s$^{-1}$ for a 0.5 keV plasma. As with Table 3, we also flag the photometric variables identified by Bonanos (2007) in Col. 6. Note that list is incomplete due to WR J and K being too close to nearby X-ray sources for meaningful limits to be determined.

| ID | Spectral Type | RA | Dec | $C_{net}$ | Var.? |
|----|------|-----|-----|------|------|
| 4 | F2Ia$^+$ | 251.75592 | −45.84364 | <4.3 | A |
| 7 | B5Ia$^+$ | 251.76508 | −45.83728 | <5.9 | A |
| 8 | F5Ia$^+$ | 251.76996 | −45.84025 | $6.8^{+6.0}_{-5.9}$ | A |
| 12 | A5Ia$^+$ | 251.75922 | −45.84967 | <3.6 | A |
| 16 | A2Ia$^+$ | 251.77754 | −45.84503 | <3.7 | A |
| 20 | <M6I | 251.76958 | −45.85661 | <5.0 | A |
| 26 | <M6I | 251.77251 | −45.84347 | <5.5 | |
| 32 | F5Ia$^+$ | 251.76529 | −45.84542 | <6.3 | |
| 33 | B5Ia$^+$ | 251.76717 | −45.84675 | <7.0 | A |
| 42 | B5Ia$^+$? | 251.76353 | −45.84781 | <4.1 | A |
| 57 | B3Ia | 251.75563 | −45.86267 | <5.8 | A |
| 70 | B3Ia | 251.78900 | −45.84711 | <5.6 | A |
| 71 | B3Ia | 251.78517 | −45.84703 | <4.4 | A |
| 75 | <M6I | 251.78667 | −45.83289 | <5.3 | |
| 237 | <M6I | 251.76286 | −45.87189 | <4.7 | A |
| 243 | LBV | 251.78146 | −45.87458 | $7.0^{+5.5}_{-5.8}$ | A |
| 265 | F5Ia$^+$ | 251.77608 | −45.82325 | < 3.7 | A |
| C | WC9d | 251.76833 | −45.85106 | <7.9 | |
| H | WC9d | 251.76708 | −45.85556 | <6.4 | |
| I | WN8o | 251.75696 | −45.85553 | <6.6 | |
| M | WC9 | 251.76649 | −45.86042 | <8.1 | |
| P | WN8 | 251.75626 | −45.86250 | <5.5 | |
| Q | WN6o | 251.73084 | −45.85944 | $6.3^{+5.8}_{-4.7}$ | |
| S | WN10-11h | 251.76237 | −45.83875 | $4.0^{+5.3}_{-3.7}$ | A |
| T | WC9d | 251.69292 | −45.79944 | <6.4 | A |
| V | WN8o | 251.76588 | −45.84408 | $22.0^{+9.0}_{-9.0}$ | |
| X | WN5o | 251.80875 | −45.80888 | $6.0^{+5.0}_{-4.0}$ | |

WR A & B show unambiguous signatures of binarity (spectroscopic and photometric, respectively). Of the 8 WC stars, 6 are found to have an IR excess, while the apparently dust free star WR E is an X-ray source, suggesting a binary fraction of ≳88%. Thus we find a lower limit to the total WR binary fraction of 70%[11] However, since some WC binaries are episodic dust makers (e.g. see Williams et al. 2005) we suspect that long-term near-IR monitoring – combined with a long term radial velocity survey – will reveal that the WR binary fraction probably approaches unity.

### 4.2. The transitional stars

The age and mass of Wd 1 results in a uniquely rich population of hot and cool transitional stars, and as such these observations represent the first systematic survey of the X-ray properties of many of these rare spectral types. The detected stars have already

been summarised in Table 3; Upper limits[12] for the remaining transitional stars are given in Table 4.

#### 4.2.1. The sgB[e] star W9

The high X-ray luminosity of W9 and the similar spectrum to WR A suggests that it too is a binary. However, unlike WR A, there is no unambiguous corroboration for a CWB identification in either the optical or radio data (Dougherty et al. 2007). An alternative explanation for the X-ray emission is accretion onto a compact companion. Two high mass X-ray binaries (HMXBs) contain sgB[e] primaries; XTE 0421+560/CI Cam and IGR J16318-4848 (e.g. Clark et al. 1999; Filliatre & Chaty 2004), both of which also demonstrate rich emission line spectra. Additionally, while not formally classified as a sgB[e] star, the spectrum of the HMXB SS433 also shows line emission of comparable strength to W9, along with an IR excess attributable to hot dust (e.g. Clark et al. 2007). In such a scenario the low luminosity and lack of variability evidenced by W9 might be explained by the observations coinciding with the long periods of X-ray quiescence between short lived outbursts exhibited by both CI Cam and IGR J16318-4848. Indeed the quiescent luminosity reported for CI Cam ($L_{1-10 \text{ keV}} \sim 10^{33}$ erg s$^{-1}$; Boirin et al. 2002) is directly comparable to that of W9.

However, a serious objection to such an hypothesis is the comparative lack of local extinction to the X-ray emitter within W9. Both HMXBs with a sgB[e] primary demonstrate $N_H \geq 10^{24}$ cm$^{-2}$ (e.g. Filliatre & Chaty 2004), which is attributed to the accretor being deeply embedded within the circumstellar envelope of the mass donor. Given the presence of circumstellar ejecta, and a dense outflow inferred from radio observations ($\dot{M} \sim 10^{-4}$ $M_\odot$ yr$^{-1}$: Dougherty et al. 2007) it is difficult to reconcile the presence of an accretor with the low intrinsic absorption ($N_H \sim 10^{22}$ cm$^{-2}$) unless it is in a wide orbit. However, the lack of local extinction also proves similarly problematic for a CWB identification.

Finally we note that either binary hypothesis could accommodate the high velocity outflow inferred from the optical He I profiles (Sect. A.2), which might arise from the system primary in both scenarios (cf. $\eta$ Car), an evolved, possible WR companion (CWB) or from an accretion driven outflow (cf. SS433; e.g. Clark et al. 2007). We suspect that as with $\eta$ Car, a combination of high spatial resolution spectroscopy and long term monitoring will be required to establish the viability of W9 as a binary, and the nature of its putative components.

#### 4.2.2. The B hypergiants and the LBV W243

As with W9, the emission from the BIa$^+$ star W13 appears too hard to be attributed to a single star and the discovery of photometric eclipses by Bonanos (2007) provides compelling evidence for its identification as a CWB. None of the cooler B hypergiants (W7, 33 & 42) are found to be X-ray sources, while the LBV W243 is only a weak detection.

Oskinova (2005a,b) and Muno et al. (2006b) provide useful summaries of existing X-ray observations of LBVs, showing emission to vary over ~three orders of magnitude from $10^{34-35}$ erg s$^{-1}$ (the *binaries $\eta$* Car and HD 5980) to <$10^{32}$ erg s$^{-1}$ (P Cygni, the Pistol Star and FMM362). While LBVs are thought

---

[11] Of the 17 WR binary candidates, 11 are found to be photometrically variable by Bonanos (2007), whereas only one of the 7 apparently single WRs is found to be. We therefore speculate that the causes of the periodic and aperiodic variability in the WRs is related to binarity, possibly due to elipsoidal modulation and/or wind perturbation.

[12] These were obtained by searching for additional X-ray sources at the optical co-ordinates of these stars utilising the aperture photometry technique described in Sect. 2.2. For the majority of stars this resulted in upper limits to the X-ray flux, although a few sources were detected at the ~90% confidence level.

to have highly structured radiatively driven winds (Davies et al. 2005), it is likely that the relatively low terminal velocities observed in cool states ($\leq$200 km s$^{-1}$; BIa$^+$) are not high enough to generate X-ray emitting material via wind shocks in single stars, although wind velocities in the hot state ($\leq$500 km s$^{-1}$; very late WN subtype) *might* suffice (Pittard & Corcoran 2002)[13].

Moreover, due to their high densities, the winds of LBVs are likely to efficiently absorb any low energy X-ray emission generated via shocks. As an extreme example, Pittard et al. (1998) show that the column depth of the wind from $\eta$ Car can reach $N_H \sim 10^{23}$ cm$^{-2}$ during X-ray eclipse. Thus even if a luminous companion is present, an LBV (or B hypergiant) CWB may be an intrinsically faint X-ray source. Consequently we suggest that the apparent lack of X-ray emission from the hot transitional stars within Wd 1 is due to a combination of their current wind properties (low velocity, high density) and/or the lack of a binary companion, and that outside of the hot state, X-ray emission from such stars will likely signify binarity.

### 4.2.3. The A-M super/hypergiants

Achmad et al. (1997) investigated the wind properties of luminous A-G stars and found that for A SGs ($T_{eff} \sim 9500-8000$ K) the observations were well matched by radiatively driven outflows. However, the wind velocities are probably too small to yield significant X-ray emission from shock heating, explaining our non detections of W12 & 16. Unfortunately, "quiescent" wind parameters for F & G super-/hypergiants are poorly constrained, although it appears likely that despite their apparently highly structured outflows (e.g. Lobel et al. 2003), wind velocities are again likely to be insufficient to generate X-ray emitting plasma from shock heating.

An alternative source of X-ray emission might be a putative high temperature chromosphere/corona. A subset of G supergiants have long been known to be X-ray sources, with solar-like far UV spectra dominated by high excitation species indicating the presence of a high temperature chromosphere (Ayres et al. 2005, and references therein). However, compared to these "active" supergiants, a second subset of "inactive" stars show UV spectra dominated by much lower excitation species and blueshifted absorption components in the chromospheric resonance lines suggestive of the presence of a cool dense wind. High excitation lines *are* present in their far-UV spectra, although significantly weaker than in the "active" stars.

Hartmann et al. (1980) denoted these objects as "hybrid chromospheric stars" due to the apparent coexistence of both high and low temperature regions within their circumstellar environments. Subsequent X-ray observations also revealed emission from such "hybrid"' stars, although at a lower level than "active" stars of similar spectral type ($L_x/L_{bol} \sim 10^{-8}$ and $10^{-6}$ respectively; Ayres et al. 2005). The difference is attributed to absorption of the X-rays by the dense cool winds of the 'hybrid' stars, which the "active" stars lack (Ayres 2005).

However, the $\sim$G0Ib stars observed by Ayres et al. have evolved from substantially less massive stars ($\sim$5–9 $M_\odot$) than the Wd 1 YHGs, and thus it is not clear whether the latter should possess chromospheres. Observations of $\rho$ Cas are inconclusive but suggest that a *permanent* chromosphere is likely absent

(Lobel et al. 2003). Given the sensitivity of our observations, if the Wd 1 YHGs were as X-ray bright as the "active" G supergiants observed by Ayres et al. (2005) they would have been detected[14]. Hence the lack of emission in W4, 32 and 265 suggests either the absence of a chromosphere/corona of sufficient temperature to generate X-rays and/or the presence of a dense cool wind that attenuates any emission. Such a dense outflow is suggested by the detection of radio emission associated with each YHG (Dougherty et al. 2007). Clearly, the confirmation of emission associated with W8 is of considerable interest in resolving whether YHGs can support high temperature chromospheres and hence coronal X-ray emission. Interestingly, W8 has no radio detection from a putative externally ionised wind.

Finally we turn to the M type SGs within Wd 1. Such stars are known to possess a chromosphere (e.g. $\alpha$ Ori; Hartmann et al. 1984), although of such low temperature (Lobel & Dupree 2000; Dupree et al. 2005) that X-ray emission would be unexpected. In any event, the dense cool winds expected for such stars (e.g. Crowther 2003) would totally veil any putative X-ray emission from a chromosphere and hence the lack of X-ray detections for the RSGs within Wd 1 is unsurprising.

### 4.3. The OB supergiants

Following the results of Clark et al. (2005; also Sect. A.3.1) we expect *individual* OB SGs within Wd 1 to have $\sim$40 $M_\odot$ progenitors, and hence bolometric luminosities in the range $3-5 \times 10^5$ $L_\odot$. Then assuming they follow the empirical $L_x \sim 10^{-7}$ $L_{bol}$ relation we should expect them to lie on the $L_x \sim 10^{32}$ erg s$^{-1}$ locus in Fig. 5, with a hardness colour of $\sim$−0.5, appropiate for the canonical 0.6 keV expected for shock-heated material within O star winds (Feldmeier et al. 1997).

Unfortunately, the 90% completeness limit for a 0.6 keV emitter is $2 \times 10^{32}$ erg s$^{-1}$ (assuming $D = 5$ kpc and $N_H = 2 \times 10^{22}$ cm$^{-2}$), hence we are likely incomplete for emission for single OB supergiant stars. Given the lack of a complete census of OB SGs (cf. Negueruela et al. in prep.) and the potentially significant scatter in the X-ray luminosities of stars of a given bolometric luminosity (cf. NGC 3603; Moffat et al. 2002), we are currently unable to quantify the degree of incompleteness or the global X-ray properties of the population of OB supergiants detected here[15].

Moreover, due to the low count rates, uncertainties on the hardness ratio are large for photon fluxes $<10^{-6}$ cm$^{-2}$ s$^{-1}$. Nevertheless, for those sources with photon fluxes below this value we find that the majority of OB SG detections have a hardness ratio within 1$\sigma$ of $\sim$−0.5, consistent with emission from single stars. However, a handful of these sources appear significantly harder. While these most likely represent statistical outliers, if their hard X-ray spectra are confirmed they may signify either the presence of low mass pre-MS companions or that they are CWBs for which a low temperature X-ray component is absent due to the significant interstellar extinction.

---

[13] The post shock temperature is given by $T = (3/16)(m/k)v^2$, where $k$ is the Boltzmann constant, $v$ the wind velocity, and $m$ is the average particle mass. For a fully ionised plasma with solar abundances, and adopting $m = 10^{-24}$ g, $kT = 0.05$ keV for $v = 200$ km s$^{-1}$ and 0.3 keV for 500 km s$^{-1}$.

[14] Assuming $\log(L_{bol}/L_\odot) \sim 5.7$ for the YHGs, and $L_x/L_{bol} \sim 10^{-6}$ yields $L_x \sim 2 \times 10^{33}$ erg s$^{-1}$. For a $10^7$ K thermal plasma – as found for $\beta$ Dra by Ayres et al. (2005) – and $D = 5$ kpc and $N_H = 2 \times 10^{22}$ cm$^{-2}$, we may derive a detection limit of $\sim$5 $\times 10^{31}$ erg s$^{-1}$ for our current observations.

[15] At an age of 4–5 Myr one would not expect Main Sequence stars earlier than $\sim$O7 V to be present in Wd1. Assuming $\log L/L_\odot \sim 5.17$ for such stars (Crowther 2003) implies, via $L_x \sim 10^{-7}$ $L_{bol}$, a corresponding X-ray flux of $\sim$6$\times 10^{31}$ erg s$^{-1}$; consequently we do not expect to detect the OB Main Sequence population of Wd 1 in our current observations.

Only eight OB SGs have photon fluxes in excess of $10^{-6}$ cm$^{-2}$ s$^{-1}$. Four of these (W24, 30a, 47 and X-1) appear to have spectra significantly harder ($\gtrsim 1.4$ keV) than 0.6 keV, while the luminosities of four of them (W27, 30a, 36 and 53) are at least an order of magnitude larger than expected from a single star. Hence we believe all to be strong binary candidates, noting that Oskinova (2005a) argues that CWBs need not always be hard sources if their emission is dominated by the intrinsic flux of both component stars, rather than the wind collision zone.

Of these objects, optical spectroscopy reveals W30a to be an interacting binary (Sect. A.3), while Bonanos (2007) finds W36 to be an eclipsing binary and W53 to be a periodic (1.3 day) photometric variable, for which it is tempting to attribute the behaviour to ellipsoidal modulation in a close binary. Moreover, both W24, and 27 have bolometric luminosities significantly in excess of that expected for single cluster SGs (with low S/N spectra of W27 hinting at binarity; Sect. A.3).

However, a number of stars for which optical spectroscopic (W6, 10, 31, 34 and 238; Sect. A.3 and Negueruela et al. in prep.), photometric (W52; Bonanos et al. 2007) or radio (W16b and W17; Dougherty et al. 2007) observations indicate (possible) binarity have X-ray properties consistent with emission from single stars, or lack detections. This could result from their winds not reaching terminal velocity, leading to systematically weaker shocks and/or the colliding wind region being deeply embedded in the X-ray photospheres of the stars, resulting in detectable hard X-ray emission only along preferred lines of sight.

Conversely, the limited temporal resolution of our current observations limits our ability to detect putative binaries spectroscopically, while a binary composed of a supergiant+MS star, would likely escape photometric detection. Thus we suspect that stars with excessive hard X-ray emission such as W47 may be confirmed as binaries upon further investigation.

The fact that the WRs are harder and more luminous in X-rays than the OB SGs (Fig. 5) can be explained by a combination of binary and stellar evolution. The increase in mass-loss rates and wind velocity as the star evolves from mid-O MS→WR will lead to greater X-ray emission from a wind-collision region, while the mass loss and/or quasi-conservative mass transfer in a close binary will act to increase the orbital separation, reducing the effects of wind opacity.

Lastly, we comment on the distribution of the spectral types of the X-ray emitters, and the apparent lack of emission from stars later than ∼B0.5Ia. Utilising an exospheric approximation, Owocki & Cohen (1999) show that the X-ray emission naturally scales as a function of the wind-density parameter ($\dot{M}/v_\infty$), rather than the canonical $L_x/L_{bol}$ relation. Given that one would naturally expect $\dot{M}/v_\infty$ to vary with spectral type, our observations support this assertion; assuming evolution at ∼const. $L_{bol}$ during the OB supergiant phase, one would not expect a dependance of the X-ray flux on spectral type – as we find – if emission solely scaled with $L_{bol}$. While beyond the scope of this work, tailored non-LTE model atmosphere analysis of both the X-ray emitting and non-emitting members of Wd 1 should allow this hypothesis to be investigated.

## 5. Low mass pre-main sequence stars

The final stellar X-ray emitters to be considered within Wd 1 are the low mass, pre-MS stars, where magnetic reconnection events produce high temperature ($T \sim 10$ MK) plasma, resulting in hard, variable X-ray emission with peak fluxes of ∼$10^{32}$ erg s$^{-1}$ (see e.g. Feigelson & Montmerle 1999). Clearly, the properties of the X-ray point sources without counterparts are consistent

with these expectations, as is the fact that counterparts to this population must be fainter than $Ks \sim 16$ mag. Conversion of this limit to a stellar mass requires accurate fitting of theoretical isochrones. Such an analysis is currently underway and will be presented in a future paper (Brandner et al. 2007). However *preliminary* results suggest that such a magnitude likely corresponds to stars of <1.5 $M_\odot$, which at an age of ∼4 Myr would correspond to stars that have still to evolve onto the ZAMS.

Utilising the findings of the *Chandra* Orion Ultradeep Project (Feigelson et al. 2005), in principle we can estimate the underlying population of pre-MS stars required to yield the X-ray bright population we detect. To accomplish this, we first define a statistically meaningful sample of sources that are bright enough to detect at least 90% of the time. For a $kT > 1$ keV plasma spectrum we require $F_X > 8.2 \times 10^{-7}$ ph cm$^{-2}$ s$^{-1}$, which corresponds to $L_X > 3 \times 10^{31}$ erg s$^{-1}$ for $D = 5$ kpc and $N_H = 2 \times 10^{22}$ cm$^{-2}$. Using this criterion, we find 45 candidate pre-MS stars within 5′ of the cluster core[16].

Preibisch & Feigelson (2005) report that X-ray emission in young low-mass stars decreases with age *at least* as rapidly as $\tau^{-0.3}$. Thus, correcting for the greater age of Wd 1 relative to Orion, we find the emission will have declined by a factor of at least 1.5. Therefore, our X-ray bright pre-MS sample within Wd 1 corresponds to the pre-MS stars within Orion with $L_X \gtrsim 5 \times 10^{31}$ erg s$^{-1}$ and $M < 1.5$ $M_\odot$. Getman et al. (2005) find only 2 of the 1616 pre-MS stars within Orion to potentially satisfy these criteria. Therefore, we conclude that the 45 X-ray bright pre-MS candidates within Wd 1 could form the high luminosity tail of a population of more than 36 000 pre-MS stars.

In principle one can estimate the pre-MS population of Wd 1 via a similar analysis of the subset of time variable objects. Within 5′ of the core of Wd 1 there are 19 pre-MS candidates with X-ray fluxes that vary between observations, 10 that exhibit flares within an observation, and 3 that exhibit both. Scaling the results of Favata et al. (2005) for Orion to both the greater distance and extinction to Wd 1, as well as the relative duration of the observations, we expect up to ∼0.1% of the pre-MS stars within Wd 1 to produce detectable flares, yielding an underlying population of ∼32 000 pre-MS stars. We caution that this is likely to be an underestimate, given that we have been forced to assume that the properties of the flares in the 1 Myr-old Orion and 4 Myr-old Wd 1 populations are identical. However, since flaring is a manifestation of the same magnetic activity that yields the quiescent X-ray flux, it is reasonable to suspect that it too will show a time dependent decay in duration, frequency or flux. Therefore, we conclude that we are currently only detecting a very small subset of the total low mass stellar population of Wd 1, and that in combination with near-IR data, deeper X-ray observations will allow a statistically robust investigation of the evolution of magnetic activity in low mass pre-MS stars.

## 6. The binary fraction of Wd 1 in context

A synthesis of the datasets described above with the study of Bonanos (2007) suggests the presence of ≥15 OB supergiant and ≥17 WR binaries within Wd 1. Given that the census of OB SGs within Wd 1 is currently incomplete, we refrain from attempting to determine a binary fraction for such stars, but find a value of ≳70% for WRs. Given that this has been inferred from a single epoch of X-ray/IR/radio observations, we suspect the true

---

[16] Within the 5′ × 5′ field previously considered we find 31 such sources.

binary fraction likely approaches unity. Moreover, since such binary signifiers are reliant on the presence of a colliding-wind region, we may also infer the presence of a massive companion for each star. For a somewhat arbitrary B0.5V companion[17] this would result in a binary mass ratio $M/M_{WR} \geq 0.4$.

Given the constraints that the binary fraction places on the physics of star formation, much effort has been expended on observational determinations of this parameter, typically via direct imaging and radial velocity surveys. For OB stars, such studies demonstrate that the binary fraction for field stars is lower than for cluster/OB association members (Mason et al. 1998), with surveys of clusters/OB associations such as NGC 6231 (Garcia & Mermilliod 2001), Cyg OB2 (Kobulnicky et al. 2006) and Sco OB2 (Kouwenhoven 2006) supporting remarkably high binary fractions ($\geq 0.6$).

Unfortunately, such studies are subject to uncertainties due to both selection effects, such as a bias towards the identification of short period systems in radial velocity surveys, and also the small sample sizes for massive stars. In the latter respect, the results for the WR population of Wd1 are significant given both the mass of the progenitors ($>45~M_\odot$: Crowther et al. 2006) and the sample size (e.g. 4 such stars within Cyg OB2 versus 24 within Wd 1). They also mirror the recent results for the 11 WC stars in the Quintuplet cluster, which appear to have a binary fraction of ~unity (Tuthill et al. 2006). Clearly, however, the applicability of these results to the wider population of massive stars requires that the WR stars would have evolved to such a state without the presence of a binary companion – i.e. that we are not introducing a selection effect by sudying this subset of the massive stellar population of these clusters.

Tuthill et al. (2006) suggest that the different ratios of WN:WC stars in the Quintuplet and Wd1 may result from binary interaction. Crowther et al. (2006) discuss the effect of binarity on this ratio, and find that current theoretical predictions for both single and binary star evolution provide a poor match to the observed ratio for Wd1. Nevertheless, they are able to show that the masses of the hydrogen deficient WRs within Wd1 are in line with expectations from single field stars and hence show no evidence for significant binary mediated mass loss. Moreover, while such a WR binary fraction in both clusters is higher than that observed for the field populations of the Galaxy (van der Hucht 2000), LMC and SMC (Foellmi 2003a, 2003b) it should be noted that the last three studies suffer from incompleteness and/or observational biases introduced by the limited temporal sampling and resolution of radial velocity surveys. Additionally, the finding of a higher binary fraction amongst cluster rather than field WRs mirrors the result of Mason et al. (1998) for galactic OB stars, which has been attributed to binary disruption due to SNe and gravitational interactions.

Thus, we consider Wd 1 and the Quintuplet cluster to provide the strongest case to date for a binary fraction approaching unity for massive stars, with initial mass $M \geq 45~M_\odot$. As such, these results are of particular interest given the possibility that the binary frequency increases with the mass of primary (e.g. Larson 2001).

As described by Kobulnicky et al. (2006), a high binary fraction for massive stars has important consequences for the identity of the progenitor populations and production rates of types Ib/c and II SNe, GRBs, X-ray binaries and binary NS systems. Moreover, if these results may be extended to lower mass stars, the binary mass ratio inferred above would likely present

significant difficulties for the production of low mass X-ray binaries via a classical scenario invoking a pre-SN binary with an extreme mass ratio, instead favouring the alternative pathway advanced by Podsiadlowski (2002) which invokes an intermediate, rather than low mass, secondary (Kobulnicky et al. 2006).

To these topics we may potentially add the production of magnetars via high mass progenitors. Crowther et al. (2006) suggest initial masses for the WN and WC stars in Wd 1 of ~45−50 and ~50−55 $M_\odot$ respectively, implying a progenitor mass of $\geq 55~M_\odot$ for the magnetar candidate. Such an estimate also appears consistent with the progenitor mass inferred for SGR 1806-20 from the properties of the host cluster, following a likely downwards revision of the distance, and hence mass of the cluster members (e.g. Figer et al. 2005; Crowther et al. 2006). Given the reduction in WR mass-loss rates when wind clumping is considered (e.g. Nugis & Lamers 2000) it seems likely that both SGR 1806-20 and CXO J164710.2-455216 formed via close binary evolution in order to arrive at a sufficiently low pre-SN core mass to result in the formation of a NS rather than a BH (e.g. Fryer et al. 2002). If correct, the reduced mass-loss rate models for the 60 $M_\odot$ primary close binary system considered by Fryer et al. (2002; their 1s2-1s4 models) form attractive progenitor templates, assuming binary disruption at SN.

However, we caution that this does not appear to be the sole channel for the formation of magnetars. Specifically, applying the the recent results of Levesque et al. (2005) to the M5 supergiants in the host cluster of SGR 1900+14 (Vrba et al. 1996, 2000) yields upper limits to their bolometric luminosities of $\log(L/L_\odot) \leq 5.0$ and 4.8, and progenitor masses of ~15 $M_\odot$ (with an uncertainty of a few solar masses due to the effect of rotation; Meynet & Maeder 2003). Given that it is not expected that stars of such low mass will evolve through a WR phase, these are likely to be the most evolved stars within the cluster. Under the hypothesis that the magnetar formed recently (e.g. Thompson et al. 2000) this implies that the progenitor of SGR 1900+14 was of significantly lower mass than either SGR 1806-20 or CXO J164710.2-455216. Indeed, such a lower limit is consistent with the formation of a neutron star from a single star without recourse to binary mediated mass loss. *Therefore, we suggest that magnetars are able to form from stars with a wide range of initial masses and that the constraints on progenitor mass presented above do not require their formation solely via a binary channel.*

## 7. Accretion onto relativistic objects

The lifetime of very massive stars is expected to asymptotically approach ~3 Myr, so with an age in the range 4−5 Myr, Wd 1 is likely to have played host to a number of SN already; indeed the presence of the magnetar CXO164710.2-455216 proves that at least one SNe has occurred and relativistic object production has commenced. However, we are currently unable to unambiguously identify any X-ray sources in Wd 1 with accreting relativistic objects.

### 7.1. Stellar mass accretors

Empirically, X-ray luminosities from HMXBs range from ~$10^{32}−10^{39}$ erg s$^{-1}$, depending on the mode of mass transfer (e.g. Negueruela 2004). With the exception of WR A, W9, W30a and W36 where the X-ray fluxes are consistent with CWBs, no other sources in Wd 1 are found to approach such fluxes. A deficit of very bright ($\geq 10^{38}$ erg s$^{-1}$) sources is likely due to the short lifetime (~$10^4$ yr) of sources fuelled by Roche

---

[17] The least massive star currently identified as a WR companion (Oskinova et al. 2005a).

Lobe overflow, while Wd 1 is too young to have yielded any classical Be/X-ray binaries. However, OB supergiant or main-sequence HMXBs emitting via direct wind-fed accretion are viable. Indeed, assuming a Kroupa type *Initial* Mass Function (Kroupa 2001), we estimate that $\sim 10^2$ stars $>50\ M_\odot$ have already been lost to SNe. Together with a binary fraction potentially approaching unity (Sect. 6), conditions within Wd 1 would apparently support their production. Observationally, such binaries are persistent sources with $L_x \sim 10^{33}$–$10^{36}$ erg s$^{-1}$ although it seems likely that the lower limit is subject to selection effects. Such bright, persistent systems should be detectable in our data, but appear to be absent.

Several reasons for this observation suggest themselves. While $\sim 10^2$ relativistic objects may have formed within Wd 1, the high binary mass fraction inferred for the WRs (Sect. 6) raises the possibility that a significant percentage of these may have been born in systems with components of $\sim$comparable mass and hence *both* stars will have already undergone SN and thus will not be available to form HMXBs at the current epoch. Alternatively, the SN may have resulted in the disruption of the binary or a post-SN configuration yielding low accretion rates and/or a short duty cycle[18]. Indeed, the role of a SN kick in a massive binary is a matter of considerable ongoing debate (e.g. Pfahl et al. 2002), with recent Monte Carlo simulations by Dray et al. (2005) demonstrating that different kick prescriptions may yield post-SN binary fractions ranging from 0.2%–40.2%, with a large number of surviving binaries having orbital parameters that preclude significant mass accretion onto the relativistic companion. Moreover, van den Heuvel et al. (2000) find a mean tangental velocity of $42 \pm 14$ km s$^{-1}$ for SG HMXBs imparted by the SN kick. This is above the likely cluster escape velocity for Wd 1 of 15 km s$^{-1}$ (Clark et al. 2005) and so it is not clear that any putative SG HMXB will remain bound within the cluster.

A final consideration is the post-SN merger of close binaries, due to either an (un?)favourably directed SN kick or the post-MS evolution of the primary leading to the spiral-in of both components and the formation of a Thorne-Zytkow object (TZO). Given that Dray et al. (2005) suggest that $\sim 1\%$ of SNe kicks may result in the production of TZOs, our above estimate of $\sim 100$ SNe to date and the presence of four highly luminous RSGs within Wd 1, it would be of interest to search these for the abundance anomalies predicted for TZOs (e.g. the $^{30}Si/^{28}Si$ ratio) by van Paradijs et al. (1995).

### 7.1.1. An intermediate mass Black Hole?

Another potential relativistic accretor within Wd 1 is an IMBH, produced by runaway coalescence of cluster members (Miller & Hamilton 2002, Portegies Zwart et al. 2004). The lack of any ultra-luminous X-ray (ULX) sources associated with Wd 1 demonstrates that it does not contain an IMBH in a close binary. For an IMBH in the cluster MGG-11 in M 82, Hopman et al. (2004; priv. comm.) estimate a companion capture event rate of only 0.05 Myr$^{-1}$. Thus, if this analysis is applicable to Wd 1 it is perhaps unsurprising that no ULX is observed, given its relative youth.

---

[18] Recently, Negueruela et al. (2005) have identified a subset of transient supergiant HMXBs with extremely short duty cycles. Given observed upper limits to the quiescent X-ray flux of $10^{32}$–$10^{33}$ erg s$^{-1}$, such a putative binary may have escaped detection if not undergoing a flare at the time of the observations. Consequently, the close similarity between the H$\alpha$ variability observed in W30a, and that seen for the SFXTs AX J1841.0-0536 and 1845.0-0433 (Negueruela et al. 2005) is particularly intriguing.

Alternatively, an IMBH might accrete from the intercluster medium. The largest rate at which we would expect an isolated black hole to accrete is the Bondi value (e.g. Frank et al. 1995): $\dot{M}_{Bondi} = 4\pi(GM)^2\rho c_s^{-3}$. Assuming that the matter emits half of its energy until it reaches the innermost stable orbit, $6GM/c^2$, the X-ray luminosity will be at most

$$\begin{aligned} L_X &= \frac{1}{12}\dot{M}_{Bondi}c^2 \\ &= 3\times 10^{29}\left(\frac{M}{100\ M_\odot}\right)^2\left(\frac{n}{1\ cm^{-3}}\right)\left(\frac{c_s}{1000\ km\ s^{-1}}\right)^{-3}\ erg\ s^{-1}, \end{aligned} \quad (3)$$

where $M$ is the mass of the black hole, $\rho$ and $n$ are the mass and number density, $c_s$ is the sound speed of the diffuse plasma. Based on the temperature of the diffuse X-ray emission, we estimate that the typical sound speed in the cluster is $c_s = 900(kT/3\ keV)^{1/2}$ km s$^{-1}$. Therefore, an intermediate mass black hole would only be detectable above our flux limit of $\sim 10^{32}$ erg s$^{-1}$ if it were particularly massive ($M \gtrsim 2000\ M_\odot$), or if it were accreting from cool, dense material (e.g., $n \sim 1000$ cm$^{-3}$, or $kT \sim 60$ eV). Moreover, Sgr A$^*$ is the best-studied black hole accreting from its surrounding ISM, and only emits X-rays with a luminosity $\sim 10^{-7}$ times that expected based on the Bondi accretion rate (Baganoff et al. 2003). This would result in an X-ray flux orders of magnitude below our detection threshold.

Similarly, the X-ray luminosity and radio flux density are expected to be related by (Maccarone 2004):

$$F_{5\ GHz} = 120\left(\frac{L_X}{10^{32}\ erg\ s^{-1}}\right)^{0.6}\left(\frac{M}{100\ M_\odot}\right)^{0.7}\left(\frac{D}{5\ kpc}\right)^{-2}\ \mu Jy. \quad (4)$$

Current radio observations can only place limits of $\approx 300\ \mu Jy$ at 5 GHz (Dougherty et al. 2007), and so in the absence of a stellar mass donor, any putative IMBH within Wd 1 is likely to be currently undetectable.

## 8. Concluding remarks

A deep 18+42ks *Chandra* observation has revealed a large population of X-ray point sources associated with the Young Massive Cluster Wd 1. We find an excess of sources with respect to background number counts out to $\sim 2'$ from the nominal core of Wd 1, or $\sim 3$ pc at a distance of 5 kpc. While larger than the value quoted by Clark et al. (2005), such a radius is consistent with IR spectroscopic and photometric studies of the cluster which reveal the presence of both high and low mass cluster members at comparable radii.

Within a $5' \times 5'$ field centred on Wd 1 we find that 46 X-ray sources are coincident with confirmed high mass cluster members. We report X-ray emission from WN and WC Wolf Rayets, hot transitional stars and OB supergiants earlier than $\sim$B0.5Ia, including the first detection of emission from WC9d stars. Based on the X-ray fluxes and spectral hardness ratios, we suspect that a significant fraction of these sources are binaries, and most likely CWBs, although the properties of a number of the OB supergiants do not exclude the possibility of emission from single stars. Further observations are anticipated in order to elucidate the nature of these systems.

Of the transitional stars, despite the formal confirmation of a sgB[e] classification and its association with a hard, luminous X-ray source, the physical nature of W9 is still unclear, although we strongly suspect it to be a binary. However the nature of the putative companion is still illusive; a synthesis of radio/IR/optical and X-ray data suggesting similarities with both

the HMXB SS 433 and the LBV $\eta$ Carinae. Where detected, we conclude that the X-ray emission from the closely interrelated WNVL and BIa$^+$ stars is due to binarity and that isolated stars of this type are likely to be intrinsically weak X-ray emitters.

No unambiguous detections of cool transitional stars were made. We attribute this to a lack of shocked material in their (slow?) winds and the probable absence of the hot, X-ray bright coronae/chromospheres that characterise lower luminosity stars of similar spectral type. Moreover, their dense winds, as inferred from radio observations, would likely be highly efficient at absorbing any X-ray emission even if a high temperature chromosphere were present.

We associate the remaining ~60 X-ray sources with a population of objects with $Ks > 16$ mag, which we suggest are pre-MS stars with $M \leq 1.5 M_\odot$. By comparison to the X-ray properties of the low mass stars within Orion we infer the presence of a substantial population of pre-MS stars within Wd 1. Deeper observations will provide significant constraints on the evolution of both quiescent and flaring X-ray emission from pre-MS stars, and hence magnetic activity, with time.

At an age of ~4−5 Myr, we expect ~$10^2$ SNe to have occurred within Wd 1. However, no X-ray sources have been unambiguously associated with accretion onto relativistic objects. We attribute the apparent lack of luminous HMXBs (>$10^{33}$ erg s$^{-1}$) to a combination of binary disruption at SNe, low accretion rates and/or a short duty cycle, large SNe kick velocities that efficiently eject such systems from the cluster (cf. Kaaret et al. 2004), and the loss of both components to SNe (suggested by the high binary mass ratio inferred for the WRs). Trivially, HMXBs accreting at a low rate would be indistinguishable from the CWBs based on our current dataset, and thus we cannot exclude the presence of such a putative population, although we may conclude that wind-fed HMXBs contribute little to cluster emissivity.

Similarly, the presence of an Intermediate Mass Black Hole cannot be excluded by our current observations. If one has formed in the last 1−2 Myr it is unlikely to have captured a stellar mass donor yet, and neither our radio nor X-ray observations are sensitive enough to detect emission from such an object if it is accreting from the hot intercluster medium.

The only X-ray bright relativistic object known within Wd 1 is the magnetar CXOU 164710.2-455216. We infer a comparable progenitor mass to that of SGR1806-20 (~55 $M_\odot$) and suggest that that both objects likely formed via close binary evolution. In contrast we find that the progenitor of SGR1900+14 was likely to have been significantly less massive (~15 $M_\odot$). We hypothesise that magnetars may arise from stars with a wide range of initial masses and hence potentially via both single star and binary pathways. Given the high binary fraction found for the WR population of Wd 1, we predict that YMCs may serve as productive birthsites for magnetars, and that due to their prompt emission, they might contribute significantly to the integrated X-ray luminosity of YMCs.

Globally, our results support the assertion of Oskinova (2005a) that the point source emission from YMCs decreases rapidly and monotonically with age, subject to possible contributions from magnetars after 3 Myr and classical Be/X-ray binaries from ~10 Myr. van den Heuvel (2000) show Be/X-ray binaries to have a mean runaway velocity comparable to the escape velocity of Wd 1, and hence may be retained within the cluster.

Lastly, we highlight that both the high binary fraction (≳70%) and mass ratio ($M/M_{WR} \geq 0.4$) inferred for the WRs within Wd 1. In conjunction with similar results for the WC stars within the Quintuplet cluster, they place the most stringent

constraints on the binary properties of massive (≥45 $M_\odot$) stars to date. While we caution that they may not be directly applicable to stars forming in less extreme environments such as loose OB associations, they are of interest for a wide range of astrophysical topics such as massive star (and star cluster) formation, the production rates of type Ib/c and type II SNe, GRBs, high and low mass X-ray binaries, magnetars and binary NS systems. In particular, if replicated for lower mass stars they would appear to heavily favour production of LMXBs via the intermediate mass channel of Podsialowski et al. (2002). Clearly, an accurate determination of the binary population of Wd 1 and their orbital properties is of great interest and consequently we are currently undertaking a combined photometric and spectroscopic investigation to elucidate these parameters.

## References

Abacete Colombo, J. F., Mendez, M., & Morrell, N. I. 2003, MNRAS, 346, 704
Achmad, L., Lamers, H. J. G. L. M., & Pasquini, L. 1997, A&A, 320, 196
Arnaud, K. A. 1996, Astronomical Data Analysis Software and Systems V, ed. G. Jacoby, & J. Barnes, ASP Conf. Ser., 101, 17
Ayres, T. R. 2005, ApJ, 618, 493
Ayres, T. R., Brown, A., & Harper, G. M. 2005, ApJ, 627, L53
Baganoff, F. K., Maeda, Y., Morris, M., et al. 2003, ApJ, 591, 891
Boirin, L., Parmar, A. N., Oosterbroek, T., et al. 2002, A&A, 394, 205
Bonanos, A. Z. 2007, AJ, submitted [arXiv:astro-ph/0702614]
Buccheri, R., Bennett, K., Bignami, G. F., et al. 1983, A&A, 128, 245
Borkowski, K. J., Lyerly, W. J., & Reynolds, S. P. 2001, ApJ, 548, 820
Brandner, W., Clark, J. S., Stolte, A., et al. 2007, A&A, accepted [arXiv:0711.1624]
Cash, W. 1979, ApJ, 228, 939
Clark, J. S., & Negueruela, I. 2002, A&A, 396, L25
Clark, J. S., Fender, R. P., Waters, L. B. F. M., et al. 1998, MNRAS, 299, L43
Clark, J. S., Steele, I. A., Fender, R. P., & Coe, M. J. 1999, A&A, 348, 888
Clark, J. S., Negueruela, I., Crowther, P. A., & Goodwin, S. P. 2005, A&A, 434, 949
Clark, J. S., Barnes, A. D., & Charles, P. A. 2007, MNRAS, 380, 263
Cheng, K. S., Taam, R. E., & Wang, W. 2004, ApJ, 617, 480
Crowther, P. A. 2003, in Evolution of Massive Stars, Mass Loss and Winds, EAS Publ. Ser., 2004, ed. M. Heydari-Malayeri, Ph. Stee, & J.-P. Zahn, 13, 119
Crowther, P. A. 2005, in Massive Star Birth: A Crossroads of Astrophysics, ed. R. Cesaroni, E. Churchwell, M. Felli, & C. Walmsley, Proc. IAU Symp., 227
Crowther, P. A., Hadfield, L. J., Clark, J. S., Negueruela, I., & Vacca, W. D. 2006, MNRAS, 372, 1407
Cutri, R. M., et al. 2003, Explanatory Supplement to the 2MASS All Sky Data Release
Davies, B., Oudmaijer, R. D., & Vink, J. S. 2005, A&A, 439, 1107
Dougherty, S. M., Clark, J. S., Waters, L. B. F. M., et al. 2007, A&A, in prep.
Dray, L. M., Dale, J. E., Beer, M. E., Napiwotzki, R., & King, A. R. 2005, MNRAS, 364, 59
Dupree, A. K., Lobel, A., Young, P. R., et al. 2005, ApJ, 622, 629
Ebisawa, K., Maeda, Y., Kaneda, H., & Yamauchi, S. 2001, Science, 293, 1633
Favata, F., Flacconio, E., Reale, F., et al. 2005, ApJS, 160, 469
Feigelson, E. D., & Montmerle, T. 1999, ARA&A, 37, 363
Feigelson, E. D., Getman, K., Townsley, L., et al. 2005, ApJS, 160, 379
Feldmeier, A., Puls, J., & Pauldrach, A. W. A. 1997, A&A, 322, 878

Figer, D. F., Najarro, F., Geballe, T. R., Blum, R. D., & Kudritzki, R. P. 2005, ApJ, 622, L49

Filliatre, P., & Chaty, S. 2004, ApJ, 616, 469

Foellmi, C., Moffat, A. F. J., & Guerrero, M. A. 2003a, MNRAS, 338, 360

Foellmi, C., Moffat, A. F. J., & Guerrero, M. A. 2003b, MNRAS, 338, 1025

Frank, J., King, A., Raine, D. 1995, Accretion Power in Astrophysics (Cambridge University Press)

Freeman, P. E., Kashyap, V., Rosner, R., & Lamb, D. Q. 2002, ApJS, 138, 185

Fryer, C. L., Heger, A., Langer, N., & Wellstein, S. 2002, ApJ, 578, 335

Garcia, B., & Mermilliod, J. C. 2001, A&A, 368, 122

Gehrels, N. 1986, ApJ, 303, 336

Getman, K. V., et al. 2005, ApJS, 160, 319

Groh, J. H., Damineli, A., Teodoro, M., & Barbosa, C. L. 2006, A&A, 457, 591

Hartmann, L., & Avrett, E. H. 1984, ApJ, 284, 238

Hartmann, L., Dupree, A. K., & Raymond, J. C. 1980, ApJ, 236, L143

Hong, J., van den Berg, M., Schlegel, E. M., et al. 2005, ApJ, 635, 907

Hopman, C., Portegies Zwart, S. F., & Tal, A. 2004, ApJ, 604, L101

Kaaret, P., Alonso-Herrero, A., Gallagher, J. S., et al. 2004, MNRAS, 348, 28

Kraft, R. P., Burrows, D. N., & Nousek, J. A. 1991, ApJ, 374, 344

Kobulnicky, H. A., Fryer, C. L., & Kiminki, D. C. 2006 [arXiv:astro-ph/0605069]

Kouwenhoven, M. B. N. 2006, Ph.D. Thesis [arXiv:astro-ph/0610792]

Kroupa, P. 2001, MNRAS, 322, 231

Lamers, H. J. G. L. M., Zickgraf, F.-J., de Winter, D., et al. 1998, A&A, 340, 117

Larson, R. B. 2001, IAU Symp., 200, 93

Law, C., & Yusef-Zadeh, F. 2004, ApJ, 611, 858.

Levesque, E. M., Massey, P., Olsen, K. A. G., et al. 2005, 628, 973

Liedahl, D. A., Osterheld, A. L., & Goldstein, W. H. 1995, ApJ, 438, L115

Lobel, A., & Dupree, A. K. 2000, ApJ, 545, 454

Lobel, A., Dupree, A. K., Stefanik, R. P., et al. 2003, ApJ, 583, 923

Long, K. S., & White, R. L. 1980, ApJ, 239, L65

Lucy, L. B., & White, R. L. 1980, ApJ, 241, 300

Lyons, L. 1991, A Practical Guide to Data Analysis for Physical Science Students (Cambridge: Cambridge Univ. Press)

Maccarone, T. J. 2004, MNRAS, 351, 1049

Mason, B. D., Gies, D. R., Hartkopf, W. I., et al. 1998, AJ, 115, 821

Mereghetti, S., Tiengo, A., Stella, L., et al. 2004, ApJ, 608, 427

Mewe, R., Gronenschild, E. H. B. M., & van den Oord, G. H. J. 1985, A&AS, 62, 197

Mewe, R., Lemen, J. R., & van den Oord, G. H. J. 1986, A&AS, 65, 511

Meynet, G., & Maeder, A. 2003, A&A, 404, 975

Miller, M. C., & Hamilton, D. P. 2002, MNRAS, 330, 232

Monet, D. G., Levine, S. E., Canzian, B., et al. 2003, AJ, 125, 984

Moffat, A. F. J., Corcoran, M. F., Stevens, I. R., et al. 2002, ApJ, 573, 191

Muno, M. P., Clark, J. S., Crowther, P. A., et al. 2006a, ApJ, 636, L41

Muno, M. P., Bower, G. C., Burgasser, A. J., et al. 2006b, ApJ, 638, 183

Muno, M. P., Law, C., Clark, J. S., et al. 2006c, ApJ, 650, 203

Muno, M. P., Gaensler, B. M., Clark, J. S., et al. 2007, MNRAS, 378, L44

Negueruela, I. 2004, in The Many Scales of the Universe - JENAM 2004 Astrophysics Reviews (Kluwer Academic Publishers), ed. J. C. del Toro Iniesta et al. [arXiv:astro-ph/0411759]

Negueruela, I., & Clark, J. S. 2005, A&A, 436, 541

Negueruela, I., Smith, D. M., Reig, P., Chaty, S., & Torrejon, J. M. 2005, in The X-ray Universe 2005, ESA-SP 604 [arXiv:astro-ph/0511088]

Nilakshi, S. R., Pandey, A. K., & Mohan, V. 2002, A&A, 383, 153

Nugis, T., & Lamers, H. J. G. L. M. 2000, A&A, 360, 227

Oskinova, L. M. 2005a, MNRAS, 361, 679

Oskinova, L. M. 2005b, in Procs. of Massive Stars and High-Energy Emission in OB Associations, ed G. Rauw, Y. Naze, R. Blomme, & E. Gosset, 99

Oskinova, L. M., Ignace, R., Hamann, W.-R., Pollock, A. M. T., & Brown, J. C. 2003, A&A, 402, 755

Owocki, S. P., & Cohen, D. H. 1999, ApJ, 520, 833

Pfahl, E., Rappaport, S., Podsiadlowski, P., & Spruit, H. 2002, ApJ, 574, 364

Piatti, A. E., Bica, E., & Clariá, J. J. 1998, A&AS, 127, 423

Pittard, J. M., Corcoran, M. F. 2002, A&A, 383, 636

Pittard, J. M., Stevens, I. R., Corcoran, M. F., & Ishibashi 1998, MNRAS, 299, L5

Podsiadlowski, Ph., Rappaport, S., & Pfahl, E. D. 2002, ApJ, 565, 1107

Pollock, A. M. T. 1987, ApJ, 320, 283

Pollock, A. M. T., Corcoran, M. F., Stevens, I. R., & Williams, P. M. 2005, ApJ, 629, 428

Portegies Zwart, S. F., Baumgardt, H., Hut Piet, Junichiro, M., & McMillan, S. L. W. 2004, Nature, 428, 724

Preibisch, T., & Feigelson, E. D. 2005, ApJS, 160, 390

Rockefeller, G., Fryer, C. L., Melia, F., & Wang, Q. D. 2005, ApJ, 623, 171

Seward, F. D., & Chlebowski, T. 1982, ApJ, 256, 530

Skinner, S. L., Simmons, A. E., Zhekov, S. A., et al. 2006, ApJ, 639, L35

Smith, N., Davidson, K., Gull, T. R., Ishibashi, K., & Hillier, D. J. 2003, ApJ, 586, 432

Thaller, M. L. 1997, ApJ, 487, 380

Thompson, C., Duncan, R. C., Woods, P. M., et al. 2000, ApJ, 543, 340

Townsley, L. K., Broos, P. S., Feigelson, E. D., et al. 2006, AJ, 131, 2164

Tuthill, P., Monnier, J., Tanner, A., et al. 2006, Science, 313 935

van den Heuvel, E. P. J., Portegies Zwart, S. F., Bhattacharya, D., & Kaper, L. 2000, A&A, 364, 563

van Paradijs, J., Spruit, H. C., van Langevelde, H. J., & Waters, L. B. F. M. 1995, A&A, 303, L25

Vrba, F. J., Luginbuhl, C. B., Hurley, K. C., et al. 1996, ApJ, 468, 225

Vrba, F. J., Henden, A. A., Luginbuhl, C. B., et al. 2000, ApJ, 533, L17

Weisskopf, M. C., Brinkman, B., Canizares, C., et al. 2002, PASP, 114, 1

Westerlund, B. E. 1987, A&AS, 70, 311

Williams, P. M., van der Hucht, K. A., & Rauw, G. 2005, in Pocs. of Massive stars and high energy emission in OB associations, ed. G. Rauw, Y. Naze, R. Blomme, & E. Gosset, 65

Zickgraf, F.-J. 2003, A&A, 408, 257

# Online Material

**Table 1.** Catalogue of the properties of the 241 X-ray point sources detected in the 2 epochs of observations. Column 1 provides the X-ray identifier, Cols. 2 and 3 the Right Ascension and Declination of the source and Cols. 4 and 5 the angular offset from the aim point of the observations and the positional uncertainty. Columns 6−9 list the detector live time, net counts, hardness ratio (as defined in Sect. 2.4) and X-ray flux respectively, for each source. Column 10 indicates source variability, if present, on short or long timescales (as described in Sect. 2.3). Finally, Col. 11 indicates whether an X-ray source has an optical or near-IR counterpart. The source catalogues utilised are 1: Clark et al. (2005), 2: Piatti et al. (1998), 3: the 2MASS catalogue (Cutri et al. 2003) and 4: the USNO-B1.0 survey (Monet et al. 2003). Designations for optical or near-IR counterparts for sources within the 5′ × 5′ field centred on Wd1 are presented in Table 3.

| X-ray Identifier | Right Ascension | Declination | Offset (arcmin) | Uncertainty (arcsec) | Detector Live Time (ks) | Net Counts | Hardness Ratio | Flux ($10^{-7}$ ph cm$^{-2}$ s$^{-1}$) | Variable? | C'part |
|---|---|---|---|---|---|---|---|---|---|---|
| 164703.7-455058 | 251.76550 | −45.84956 | 0.0 | 0.5 | 53.7 | $27.2^{+6.1}_{-5.8}$ | $-0.15^{+0.21}_{-0.21}$ | 13.6 | | 1 |
| 164704.1-455107 | 251.76747 | −45.85195 | 0.1 | 0.5 | 53.7 | $80.8^{+9.6}_{-10.3}$ | $0.34^{+0.11}_{-0.11}$ | 48.8 | | 12 |
| 164703.6-455051 | 251.76515 | −45.84757 | 0.1 | 0.5 | 53.7 | $6.5^{+4.6}_{-5.1}$ | $1.00_{-1.17}$ | 3.1 | | 1 |
| 164703.1-455051 | 251.76306 | −45.84766 | 0.2 | 0.5 | 53.7 | $15.3^{+5.4}_{-5.4}$ | $-0.19^{+0.34}_{-0.36}$ | 7.9 | | |
| 164702.7-455057 | 251.76135 | −45.84934 | 0.2 | 0.5 | 53.7 | $14.1^{+4.6}_{-4.0}$ | $-0.21^{+0.30}_{-0.31}$ | 6.1 | | |
| 164704.4-455109 | 251.76857 | −45.85257 | 0.2 | 0.5 | 53.7 | $13.9^{+3.8}_{-4.8}$ | $0.02^{+0.31}_{-0.31}$ | 6.6 | | 1 |
| 164702.4-455100 | 251.76024 | −45.85002 | 0.2 | 0.5 | 53.7 | $22.8^{+5.2}_{-6.0}$ | $0.19^{+0.23}_{-0.24}$ | 11.4 | | |
| 164702.6-455050 | 251.76118 | −45.84731 | 0.2 | 0.5 | 53.7 | $35.6^{+6.1}_{-6.5}$ | $-0.24^{+0.17}_{-0.17}$ | 16.0 | | 12 |
| 164705.0-455055 | 251.77115 | −45.84866 | 0.3 | 0.5 | 53.7 | $43.4^{+7.2}_{-7.4}$ | $-0.79^{+0.13}_{-0.11}$ | 19.0 | | 123 |
| 164702.8-455046 | 251.76193 | −45.84617 | 0.3 | 0.5 | 53.7 | $9.0^{+4.2}_{-3.6}$ | $-0.39^{+0.41}_{-0.43}$ | 3.3 | | 1 |
| 164705.3-455104 | 251.77237 | −45.85132 | 0.3 | 0.5 | 53.7 | $237.5^{+16.1}_{-16.5}$ | $0.21^{+0.06}_{-0.07}$ | 133.2 | | 1 |
| 164703.0-455043 | 251.76277 | −45.84533 | 0.3 | 0.5 | 53.7 | $10.9^{+3.7}_{-4.9}$ | $-1.00^{+0.55}$ | 4.2 | | 1 |
| 164702.1-455112 | 251.75897 | −45.85360 | 0.3 | 0.5 | 53.7 | $19.3^{+5.4}_{-5.2}$ | $0.14^{+0.27}_{-0.27}$ | 11.9 | | 3 |
| 164703.4-455039 | 251.76456 | −45.84423 | 0.3 | 0.5 | 53.7 | $5.9^{+3.2}_{-4.3}$ | $1.00_{-1.03}$ | 4.2 | | 1 |
| 164704.1-455039 | 251.76711 | −45.84420 | 0.4 | 0.5 | 53.7 | $552.2^{+24.9}_{-24.5}$ | $-0.15^{+0.04}_{-0.04}$ | 253.4 | | 1 |
| 164704.9-455116 | 251.77077 | −45.85461 | 0.4 | 0.5 | 53.7 | $12.9^{+4.2}_{-5.3}$ | $0.52^{+0.34}_{-0.33}$ | 7.7 | | |
| 164702.5-455117 | 251.76077 | −45.85496 | 0.4 | 0.5 | 53.7 | $18.0^{+4.8}_{-6.0}$ | $0.22^{+0.30}_{-0.29}$ | 10.1 | | 123 |
| 164705.1-455041 | 251.77151 | −45.84482 | 0.4 | 0.5 | 53.7 | $32.9^{+5.8}_{-6.9}$ | $-0.72^{+0.15}_{-0.14}$ | 13.4 | | 12 |
| 164704.0-455124 | 251.76672 | −45.85694 | 0.4 | 0.5 | 53.7 | $19.2^{+5.5}_{-5.1}$ | $0.55^{+0.25}_{-0.25}$ | 17.5 | | 1 |
| 164703.3-455034 | 251.76404 | −45.84296 | 0.4 | 0.5 | 53.7 | $10.2^{+3.8}_{-3.5}$ | $-0.43^{+0.34}_{-0.32}$ | 4.2 | | 23 |
| 164706.2-455048 | 251.77600 | −45.84694 | 0.5 | 0.5 | 53.7 | $7.2^{+4.0}_{-3.8}$ | $-1.00^{+0.63}$ | 2.4 | l | 1 |
| 164704.1-455031 | 251.76724 | −45.84201 | 0.5 | 0.5 | 53.7 | $462.2^{+22.7}_{-22.4}$ | $0.23^{+0.05}_{-0.05}$ | 241.2 | | 123 |
| 164702.0-455035 | 251.75835 | −45.84329 | 0.5 | 0.5 | 53.7 | $9.0^{+3.2}_{-4.4}$ | $-1.00^{+0.32}$ | 2.7 | | |
| 164705.7-455033 | 251.77412 | −45.84261 | 0.6 | 0.5 | 53.7 | $11.2^{+4.0}_{-3.6}$ | $-1.00^{+0.36}$ | 4.9 | | 12 |
| 164706.5-455039 | 251.77725 | −45.84417 | 0.6 | 0.5 | 53.7 | $161.2^{+13.6}_{-13.2}$ | $-0.14^{+0.08}_{-0.08}$ | 81.4 | | 1 |
| 164703.7-455023 | 251.76553 | −45.83974 | 0.6 | 0.5 | 53.7 | $13.9^{+4.0}_{-5.1}$ | $0.65^{+0.26}_{-0.27}$ | 7.1 | | |
| 164703.0-455023 | 251.76271 | −45.83987 | 0.6 | 0.5 | 53.7 | $11.1^{+3.9}_{-3.3}$ | $-0.47^{+0.31}_{-0.29}$ | 4.7 | | 123 |
| 164701.6-455130 | 251.75688 | −45.85860 | 0.6 | 0.5 | 53.7 | $11.0^{+4.9}_{-4.2}$ | $1.00_{-0.29}$ | 7.1 | | |
| 164706.2-455126 | 251.77605 | −45.85740 | 0.6 | 0.5 | 53.7 | $14.3^{+4.7}_{-4.6}$ | $1.00_{-0.19}$ | 16.6 | | 1 |
| 164707.0-455042 | 251.77951 | −45.84504 | 0.7 | 0.5 | 53.7 | $9.0^{+3.1}_{-4.4}$ | $0.28^{+0.43}_{-0.41}$ | 6.1 | s | |
| 164705.7-455133 | 251.77397 | −45.85929 | 0.7 | 0.5 | 53.7 | $12.7^{+3.6}_{-4.2}$ | $-0.08^{+0.31}_{-0.31}$ | 6.7 | | 3 |
| 164702.5-455137 | 251.76045 | −45.86053 | 0.7 | 0.5 | 53.7 | $15.3^{+4.5}_{-4.3}$ | $-0.51^{+0.27}_{-0.26}$ | 6.5 | | 23 |
| 164701.2-455130 | 251.75519 | −45.85851 | 0.7 | 0.5 | 53.7 | $10.1^{+4.5}_{-3.9}$ | $1.00^{+}_{-0.16}$ | 7.6 | l | |
| 164704.5-455139 | 251.76878 | −45.86105 | 0.7 | 0.5 | 53.7 | $8.2^{+4.1}_{-3.7}$ | $0.33^{+0.48}_{-0.46}$ | 4.1 | | |
| 164704.5-455018 | 251.76898 | −45.83841 | 0.7 | 0.5 | 53.7 | $11.3^{+4.2}_{-4.1}$ | $0.15^{+0.38}_{-0.36}$ | 5.7 | | |
| 164706.6-455029 | 251.77760 | −45.84157 | 0.7 | 0.5 | 53.7 | $10.2^{+3.7}_{-3.3}$ | $-0.62^{+0.30}_{-0.28}$ | 4.5 | | 1 |
| 164702.5-455142 | 251.76067 | −45.86169 | 0.7 | 0.5 | 53.7 | $3.4^{+2.7}_{-3.0}$ | $-1.00^{+0.80}$ | 1.5 | | 1 |
| 164706.4-455026 | 251.77686 | −45.84057 | 0.7 | 0.5 | 53.7 | $18.9^{+4.1}_{-5.2}$ | $0.14^{+0.24}_{-0.24}$ | 13.1 | | 124 |
| 164706.0-455022 | 251.77528 | −45.83963 | 0.7 | 0.5 | 53.7 | $30.8^{+5.9}_{-6.8}$ | $0.27^{+0.20}_{-0.20}$ | 20.5 | | |
| 164704.2-455146 | 251.76753 | −45.86281 | 0.8 | 0.5 | 53.7 | $11.6^{+3.4}_{-3.9}$ | $0.09^{+0.31}_{-0.31}$ | 6.7 | | |
| 164703.8-455146 | 251.76619 | −45.86293 | 0.8 | 0.5 | 53.7 | $12.6^{+3.5}_{-4.0}$ | $0.47^{+0.26}_{-0.28}$ | 6.8 | | 1 |
| 164703.2-455013 | 251.76352 | −45.83702 | 0.8 | 0.5 | 53.7 | $10.6^{+3.8}_{-4.3}$ | $1.00_{-0.48}$ | 4.9 | | |
| 164659.3-455046 | 251.74742 | −45.84632 | 0.8 | 0.5 | 53.7 | $11.3^{+3.6}_{-3.6}$ | $-0.27^{+0.32}_{-0.31}$ | 4.9 | | 13 |
| 164700.3-455131 | 251.75160 | −45.85884 | 0.8 | 0.5 | 53.7 | $56.7^{+7.6}_{-8.2}$ | $-0.58^{+0.12}_{-0.11}$ | 24.0 | | 123 |
| 164708.3-455045 | 251.78479 | −45.84594 | 0.8 | 0.5 | 53.7 | $743.7^{+27.3}_{-27.3}$ | $0.19^{+0.04}_{-0.04}$ | 380.7 | | 1 |
| 164702.8-455009 | 251.76175 | −45.83610 | 0.8 | 0.5 | 53.7 | $21.0^{+4.3}_{-5.5}$ | $0.49^{+0.19}_{-0.21}$ | 11.5 | l | |
| 164701.9-455148 | 251.75813 | −45.86351 | 0.9 | 0.5 | 53.7 | $9.6^{+3.2}_{-3.7}$ | $-0.06^{+0.36}_{-0.37}$ | 4.5 | | |
| 164704.5-455008 | 251.76900 | −45.83559 | 0.9 | 0.5 | 53.7 | $14.2^{+4.2}_{-3.9}$ | $-0.42^{+0.27}_{-0.25}$ | 6.3 | | 2 |
| 164702.1-455151 | 251.75894 | −45.86440 | 0.9 | 0.5 | 53.7 | $16.4^{+4.3}_{-4.3}$ | $-0.16^{+0.26}_{-0.26}$ | 8.7 | | |
| 164658.6-455114 | 251.74454 | −45.85406 | 0.9 | 0.5 | 53.7 | $15.3^{+4.3}_{-4.1}$ | $-0.07^{+0.27}_{-0.27}$ | 7.8 | | 23 |
| 164658.9-455038 | 251.74559 | −45.84389 | 0.9 | 0.5 | 53.7 | $4.1^{+3.0}_{-2.5}$ | $-1.00^{+0.88}$ | 1.0 | | |
| 164704.6-455155 | 251.76930 | −45.86529 | 0.9 | 0.5 | 53.7 | $7.9^{+3.0}_{-4.2}$ | $-0.10^{+0.47}_{-0.47}$ | 4.7 | | |
| 164701.4-455150 | 251.75586 | −45.86411 | 0.9 | 0.5 | 53.7 | $9.9^{+3.0}_{-4.0}$ | $-0.43^{+0.34}_{-0.33}$ | 4.2 | | 1 |
| 164658.2-455056 | 251.74287 | −45.84914 | 0.9 | 0.5 | 53.7 | $12.7^{+3.5}_{-4.1}$ | $-0.18^{+0.30}_{-0.29}$ | 6.5 | | 3 |
| 164708.6-455034 | 251.78601 | −45.84283 | 1.0 | 0.5 | 53.7 | $6.7^{+3.0}_{-3.6}$ | $-0.20^{+0.49}_{-0.52}$ | 4.7 | | |
| 164659.0-455028 | 251.74606 | −45.84122 | 1.0 | 0.5 | 53.7 | $10.4^{+3.4}_{-3.5}$ | $-1.00^{+0.30}$ | 3.9 | | 123 |
| 164703.2-455157 | 251.76343 | −45.86605 | 1.0 | 0.5 | 53.7 | $18.0^{+4.0}_{-5.1}$ | $-1.00^{+0.26}$ | 7.0 | | 1 |
| 164709.0-455042 | 251.78780 | −45.84523 | 1.0 | 0.5 | 53.7 | $12.3^{+4.4}_{-4.2}$ | $1.00_{-0.28}$ | 15.9 | | |

**Table 1.** continued.

| X-ray Identifier | Right Ascension | Declination | Offset (arcmin) | Uncertainty (arcsec) | Detector Live Time (ks) | Net Counts | Hardness Ratio | Flux ($10^{-7}$ ph cm$^{-2}$ s$^{-1}$) | Variable? | C'part |
|---|---|---|---|---|---|---|---|---|---|---|
| 164707.0-455012 | 251.77950 | −45.83693 | 1.0 | 0.5 | 53.7 | $9.3^{+3.4}_{-3.2}$ | $-0.75^{+0.29}_{-0.24}$ | 4.0 | | 1234 |
| 164701.0-455006 | 251.75427 | −45.83522 | 1.0 | 0.5 | 53.7 | $14.5^{+3.9}_{-4.1}$ | $-0.43^{+0.26}_{-0.25}$ | 6.2 | | 13 |
| 164708.2-455137 | 251.78458 | −45.86048 | 1.0 | 0.5 | 53.7 | $7.3^{+3.5}_{-3.4}$ | $1.00_{-0.45}$ | 3.8 | | |
| 164709.4-455116 | 251.78935 | −45.85445 | 1.0 | 0.5 | 53.7 | $9.1^{+3.9}_{-3.4}$ | $1.00_{-0.43}$ | 7.2 | | |
| 164708.9-455029 | 251.78737 | −45.84150 | 1.0 | 0.5 | 53.7 | $8.7^{+3.2}_{-3.8}$ | $-0.09^{+0.40}_{-0.42}$ | 4.8 | | 3 |
| 164707.8-455147 | 251.78258 | −45.86306 | 1.1 | 0.5 | 53.7 | $14.5^{+3.9}_{-4.2}$ | $0.40^{+0.25}_{-0.27}$ | 7.2 | | |
| 164709.5-455040 | 251.78993 | −45.84452 | 1.1 | 0.5 | 53.7 | $12.1^{+4.3}_{-3.8}$ | $0.44^{+0.30}_{-0.31}$ | 6.1 | | |
| 164706.7-455003 | 251.77832 | −45.83443 | 1.1 | 0.5 | 53.7 | $19.9^{+4.4}_{-5.6}$ | $0.51^{+0.22}_{-0.23}$ | 10.8 | | |
| 164706.9-455157 | 251.77913 | −45.86598 | 1.1 | 0.5 | 53.7 | $10.7^{+3.7}_{-4.4}$ | $0.33^{+0.37}_{-0.37}$ | 5.4 | | |
| 164710.0-455049 | 251.79185 | −45.84722 | 1.1 | 0.5 | 53.7 | $19.9^{+4.4}_{-5.6}$ | $0.59^{+0.21}_{-0.22}$ | 11.6 | l | |
| 164709.7-455036 | 251.79079 | −45.84337 | 1.1 | 0.5 | 53.7 | $9.0^{+2.9}_{-4.1}$ | $1.00_{-0.30}$ | 4.5 | | |
| 164658.8-455145 | 251.74530 | −45.86274 | 1.1 | 0.5 | 53.7 | $14.5^{+3.9}_{-4.2}$ | $-0.02^{+0.28}_{-0.28}$ | 6.8 | | 1 |
| 164658.8-455014 | 251.74535 | −45.83722 | 1.1 | 0.5 | 53.7 | $10.0^{+3.1}_{-4.4}$ | $0.35^{+0.36}_{-0.37}$ | 5.8 | | |
| 164709.2-455024 | 251.78870 | −45.84015 | 1.1 | 0.5 | 53.7 | $4.9^{+2.2}_{-3.3}$ | $-0.11^{+0.58}_{-0.62}$ | 1.8 | | |
| 164706.9-455201 | 251.77908 | −45.86716 | 1.2 | 0.5 | 53.7 | $9.9^{+3.0}_{-4.0}$ | $-1.00^{+0.30}$ | 3.6 | | 12 |
| 164705.9-455208 | 251.77495 | −45.86890 | 1.2 | 0.5 | 53.7 | $8.0^{+4.0}_{-3.3}$ | $-0.57^{+0.39}_{-0.40}$ | 3.7 | | |
| 164707.4-454959 | 251.78125 | −45.83326 | 1.2 | 0.5 | 53.7 | $10.5^{+3.7}_{-4.1}$ | $1.00_{-0.25}$ | 6.4 | l | |
| 164657.3-455030 | 251.73892 | −45.84186 | 1.2 | 0.5 | 53.7 | $37.6^{+6.4}_{-6.8}$ | $0.47^{+0.15}_{-0.16}$ | 22.3 | sl | |
| 164659.9-454958 | 251.74998 | −45.83288 | 1.2 | 0.5 | 53.7 | $8.9^{+2.9}_{-4.0}$ | $0.61^{+0.31}_{-0.34}$ | 5.4 | | |
| 164705.6-455210 | 251.77353 | −45.86949 | 1.2 | 0.5 | 53.7 | $4.0^{+1.7}_{-2.9}$ | $-1.00^{+0.64}$ | 1.4 | l | |
| 164702.7-455212 | 251.76160 | −45.87027 | 1.2 | 0.5 | 53.7 | $12.3^{+3.8}_{-3.7}$ | $-0.02^{+0.30}_{-0.31}$ | 5.6 | | |
| 164703.4-455213 | 251.76454 | −45.87046 | 1.2 | 0.5 | 53.7 | $13.7^{+4.1}_{-4.7}$ | $0.29^{+0.33}_{-0.31}$ | 8.1 | | |
| 164659.0-455158 | 251.74585 | −45.86629 | 1.3 | 0.5 | 53.7 | $8.4^{+3.4}_{-3.5}$ | $0.42^{+0.38}_{-0.39}$ | 4.5 | | |
| 164657.2-455139 | 251.73848 | −45.86091 | 1.3 | 0.5 | 53.7 | $18.0^{+5.1}_{-4.4}$ | $0.19^{+0.25}_{-0.26}$ | 10.9 | s | |
| 164656.3-455118 | 251.73491 | −45.85508 | 1.3 | 0.5 | 53.7 | $9.9^{+3.2}_{-4.3}$ | $0.41^{+0.36}_{-0.36}$ | 6.3 | | |
| 164659.9-454951 | 251.74989 | −45.83089 | 1.3 | 0.5 | 53.7 | $9.0^{+3.8}_{-3.1}$ | $1.00_{-0.32}$ | 7.9 | | |
| 164704.4-455220 | 251.76852 | −45.87247 | 1.4 | 0.5 | 53.7 | $5.0^{+1.8}_{-3.0}$ | $-0.38^{+0.49}_{-0.45}$ | 3.4 | | |
| 164704.4-455222 | 251.76846 | −45.87304 | 1.4 | 0.5 | 53.7 | $9.1^{+3.4}_{-2.8}$ | $0.68^{+0.25}_{-0.30}$ | 7.5 | | |
| 164702.9-454935 | 251.76225 | −45.82650 | 1.4 | 0.5 | 53.7 | $9.3^{+3.7}_{-3.6}$ | $1.00_{-0.42}$ | 5.3 | l | |
| 164656.0-455029 | 251.73364 | −45.84148 | 1.4 | 0.5 | 53.7 | $12.7^{+3.8}_{-4.3}$ | $0.72^{+0.22}_{-0.26}$ | 9.7 | | |
| 164657.2-455153 | 251.73849 | −45.86491 | 1.4 | 0.5 | 53.7 | $19.7^{+4.6}_{-5.2}$ | $0.30^{+0.23}_{-0.24}$ | 15.9 | s | |
| 164705.2-455224 | 251.77167 | −45.87360 | 1.4 | 0.5 | 53.7 | $109.6^{+10.9}_{-11.3}$ | $0.63^{+0.08}_{-0.08}$ | 65.7 | | 124 |
| 164706.9-454940 | 251.77911 | −45.82779 | 1.5 | 0.5 | 53.7 | $12.6^{+3.6}_{-4.0}$ | $-0.33^{+0.29}_{-0.28}$ | 5.4 | | 12 |
| 164700.3-454940 | 251.75133 | −45.82779 | 1.5 | 0.5 | 53.7 | $9.1^{+3.7}_{-3.2}$ | $0.17^{+0.38}_{-0.39}$ | 4.5 | | |
| 164655.2-455124 | 251.73024 | −45.85678 | 1.5 | 0.5 | 53.7 | $5.6^{+2.8}_{-3.2}$ | $0.10^{+0.55}_{-0.57}$ | 3.9 | | |
| 164706.2-454931 | 251.77606 | −45.82531 | 1.5 | 0.5 | 53.7 | $9.8^{+3.2}_{-4.1}$ | $0.45^{+0.33}_{-0.35}$ | 5.7 | s | |
| 164709.2-455214 | 251.78854 | −45.87056 | 1.6 | 0.5 | 53.7 | $12.8^{+3.9}_{-4.7}$ | $-0.38^{+0.32}_{-0.31}$ | 5.0 | | |
| 164656.9-454957 | 251.73720 | −45.83272 | 1.6 | 0.5 | 53.7 | $5.2^{+3.1}_{-2.8}$ | $0.44^{+0.53}_{-0.54}$ | 3.6 | | |
| 164702.3-455233 | 251.75981 | −45.87609 | 1.6 | 0.5 | 53.7 | $9.9^{+2.8}_{-3.8}$ | $-0.54^{+0.31}_{-0.28}$ | 4.9 | | 123 |
| 164659.8-455227 | 251.74954 | −45.87420 | 1.6 | 0.5 | 53.7 | $24.1^{+5.7}_{-5.2}$ | $0.39^{+0.20}_{-0.21}$ | 15.3 | l | |
| 164654.4-455053 | 251.72679 | −45.84825 | 1.6 | 0.5 | 53.7 | $7.3^{+3.3}_{-3.3}$ | $0.32^{+0.44}_{-0.45}$ | 4.9 | | |
| 164700.9-454927 | 251.75400 | −45.82420 | 1.6 | 0.5 | 53.7 | $9.1^{+3.8}_{-3.2}$ | $0.13^{+0.37}_{-0.39}$ | 5.9 | | |
| 164709.2-454941 | 251.78842 | −45.82810 | 1.6 | 0.5 | 53.7 | $17.7^{+4.3}_{-5.0}$ | $0.36^{+0.24}_{-0.25}$ | 10.9 | l | |
| 164701.4-455235 | 251.75589 | −45.87642 | 1.6 | 0.5 | 53.7 | $11.9^{+3.1}_{-4.2}$ | $-0.25^{+0.30}_{-0.29}$ | 5.4 | | 1234 |
| 164654.6-455129 | 251.72781 | −45.85824 | 1.6 | 0.5 | 53.7 | $10.8^{+3.3}_{-4.3}$ | $1.00_{-0.42}$ | 7.9 | | |
| 164656.0-455000 | 251.73372 | −45.83334 | 1.7 | 0.5 | 53.7 | $5.8^{+2.1}_{-3.1}$ | $-1.00^{+0.49}$ | 2.5 | | 12 |
| 164701.7-455238 | 251.75739 | −45.87732 | 1.7 | 0.5 | 53.7 | $6.0^{+2.3}_{-3.6}$ | $0.43^{+0.46}_{-0.48}$ | 2.5 | | |
| 164711.5-455000 | 251.79794 | −45.83335 | 1.7 | 0.5 | 53.7 | $5.1^{+3.1}_{-2.5}$ | $1.00_{-0.49}$ | 2.3 | | 1 |
| 164654.0-455111 | 251.72533 | −45.85331 | 1.7 | 0.5 | 53.7 | $5.5^{+2.4}_{-2.8}$ | $-1.00^{+0.49}$ | 1.9 | | |
| 164710.2-455216 | 251.79250 | −45.87136 | 1.7 | 0.5 | 53.7 | $1148.9^{+33.9}_{-33.9}$ | $0.12^{+0.03}_{-0.03}$ | 607.6 | | |
| 164707.6-455235 | 251.78191 | −45.87666 | 1.7 | 0.5 | 53.7 | $54.5^{+7.7}_{-8.1}$ | $0.07^{+0.14}_{-0.14}$ | 27.0 | | 1 |
| 164707.6-454922 | 251.78174 | −45.82283 | 1.8 | 0.5 | 53.7 | $21.1^{+5.2}_{-4.8}$ | $0.72^{+0.16}_{-0.19}$ | 15.9 | | 13 |
| 164714.4-455101 | 251.81032 | −45.85046 | 1.9 | 0.5 | 53.7 | $6.0^{+3.1}_{-2.5}$ | $1.00_{-0.48}$ | 5.1 | | |
| 164654.2-455154 | 251.72603 | −45.86518 | 1.9 | 0.5 | 53.7 | $9.7^{+3.0}_{-3.6}$ | $-0.54^{+0.32}_{-0.29}$ | 6.4 | | 124 |
| 164702.8-455252 | 251.76170 | −45.88135 | 1.9 | 0.5 | 53.7 | $8.3^{+3.7}_{-3.6}$ | $0.27^{+0.43}_{-0.43}$ | 4.1 | s | |
| 164657.0-455231 | 251.73764 | −45.87528 | 1.9 | 0.5 | 53.7 | $45.2^{+7.3}_{-7.1}$ | $0.13^{+0.15}_{-0.15}$ | 25.1 | sl | |
| 164713.5-455156 | 251.80641 | −45.86556 | 2.0 | 0.5 | 53.7 | $7.4^{+3.1}_{-3.2}$ | $0.46^{+0.38}_{-0.40}$ | 5.6 | | |
| 164657.2-455235 | 251.73845 | −45.87663 | 2.0 | 0.5 | 53.7 | $55.4^{+7.9}_{-7.9}$ | $0.61^{+0.11}_{-0.12}$ | 34.4 | sl | |
| 164704.6-454902 | 251.76921 | −45.81723 | 2.0 | 0.5 | 53.7 | $8.7^{+3.2}_{-3.8}$ | $-0.13^{+0.40}_{-0.42}$ | 4.0 | s | |
| 164701.1-455256 | 251.75491 | −45.88249 | 2.0 | 0.5 | 53.7 | $18.3^{+4.5}_{-4.3}$ | $0.27^{+0.22}_{-0.24}$ | 11.9 | l | |
| 164701.0-454901 | 251.75429 | −45.81720 | 2.0 | 0.5 | 53.7 | $4.5^{+2.6}_{-2.9}$ | $1.00_{-0.82}$ | 3.2 | | 3 |
| 164701.0-455258 | 251.75432 | −45.88291 | 2.0 | 0.5 | 53.7 | $9.3^{+3.2}_{-3.1}$ | $0.84^{+0.16}_{-0.25}$ | 7.6 | | |
| 164710.8-455246 | 251.79518 | −45.87958 | 2.2 | 0.5 | 53.7 | $8.7^{+3.1}_{-3.8}$ | $0.15^{+0.39}_{-0.41}$ | 4.3 | | |
| 164651.7-455017 | 251.71567 | −45.83819 | 2.2 | 0.5 | 53.7 | $7.7^{+2.8}_{-3.5}$ | $-0.63^{+0.36}_{-0.35}$ | 3.5 | | |

**Table 1.** continued.

| X-ray Identifier | Right Ascension | Declination | Offset (arcmin) | Uncertainty (arcsec) | Detector Live Time (ks) | Net Counts | Hardness Ratio | Flux ($10^{-7}$ ph cm$^{-2}$ s$^{-1}$) | Variable? | C'part |
|---|---|---|---|---|---|---|---|---|---|---|
| 164658.8-455301 | 251.74510 | −45.88380 | 2.2 | 0.5 | 53.7 | $15.2^{+4.6}_{-4.2}$ | $0.27^{+0.27}_{-0.28}$ | 10.5 | | |
| 164706.6-455308 | 251.77789 | −45.88570 | 2.2 | 0.5 | 53.7 | $6.2^{+2.8}_{-2.4}$ | $-1.00^{+0.52}$ | 2.5 | | 1 |
| 164657.7-455300 | 251.74063 | −45.88345 | 2.3 | 0.5 | 53.7 | $25.8^{+5.0}_{-6.0}$ | $0.24^{+0.20}_{-0.21}$ | 13.8 | 1 | |
| 164653.9-455230 | 251.72485 | −45.87515 | 2.3 | 0.5 | 53.7 | $10.9^{+3.2}_{-4.3}$ | $-0.44^{+0.33}_{-0.33}$ | 4.0 | 1 | |
| 164658.5-455316 | 251.74409 | −45.88796 | 2.4 | 0.5 | 53.7 | $35.2^{+6.5}_{-6.2}$ | $0.90^{+0.08}_{-0.10}$ | 27.9 | | |
| 164655.3-455258 | 251.73058 | −45.88298 | 2.5 | 0.5 | 53.7 | $7.7^{+3.0}_{-3.6}$ | $-0.25^{+0.42}_{-0.45}$ | 2.9 | s | |
| 164706.9-454833 | 251.77898 | −45.80943 | 2.5 | 0.5 | 53.7 | $11.1^{+4.0}_{-3.6}$ | $0.64^{+0.25}_{-0.29}$ | 8.7 | | |
| 164654.8-454900 | 251.72836 | −45.81673 | 2.5 | 0.5 | 53.7 | $18.9^{+4.2}_{-5.4}$ | $0.27^{+0.23}_{-0.24}$ | 10.8 | | |
| 164652.3-454924 | 251.71808 | −45.82344 | 2.5 | 0.5 | 53.7 | $7.6^{+3.0}_{-3.6}$ | $0.03^{+0.43}_{-0.46}$ | 4.6 | | |
| 164718.1-455125 | 251.82559 | −45.85702 | 2.5 | 0.5 | 53.7 | $12.5^{+3.5}_{-3.7}$ | $-0.57^{+0.26}_{-0.22}$ | 9.0 | | 134 |
| 164718.2-455029 | 251.82587 | −45.84144 | 2.6 | 0.5 | 53.7 | $7.9^{+2.4}_{-3.5}$ | $-1.00^{+0.40}$ | 3.0 | | 1 |
| 164650.8-454943 | 251.71178 | −45.82877 | 2.6 | 0.5 | 53.7 | $30.6^{+5.8}_{-6.2}$ | $1.00_{-0.11}$ | 26.2 | 1 | |
| 164656.1-455314 | 251.73378 | −45.88729 | 2.6 | 0.5 | 53.7 | $611.2^{+25.8}_{-25.5}$ | $-0.95^{+0.01}_{-0.01}$ | 265.0 | | 34 |
| 164715.6-454924 | 251.81526 | −45.82357 | 2.6 | 0.5 | 53.7 | $7.1^{+3.1}_{-2.5}$ | $-1.00^{+0.45}$ | 3.0 | | |
| 164713.6-454857 | 251.80682 | −45.81588 | 2.7 | 0.5 | 53.7 | $113.7^{+10.9}_{-11.5}$ | $-0.57^{+0.08}_{-0.08}$ | 51.8 | 1 | 14 |
| 164705.3-455340 | 251.77243 | −45.89453 | 2.7 | 0.5 | 53.7 | $3.9^{+1.6}_{-2.6}$ | $-1.00^{+0.40}$ | 1.2 | | |
| 164654.6-455316 | 251.72775 | −45.88782 | 2.8 | 0.5 | 53.7 | $9.1^{+3.6}_{-3.0}$ | $-1.00^{+0.47}$ | 3.4 | | |
| 164658.3-455338 | 251.74315 | −45.89399 | 2.8 | 0.5 | 53.7 | $13.2^{+4.2}_{-3.9}$ | $0.24^{+0.29}_{-0.30}$ | 6.9 | | |
| 164716.9-454925 | 251.82083 | −45.82369 | 2.8 | 0.5 | 53.7 | $18.1^{+4.8}_{-4.3}$ | $0.85^{+0.12}_{-0.17}$ | 18.9 | | |
| 164651.7-454907 | 251.71550 | −45.81882 | 2.8 | 0.5 | 53.7 | $11.2^{+3.8}_{-3.5}$ | $-0.70^{+0.28}_{-0.25}$ | 5.3 | | 1 |
| 164647.8-455129 | 251.69933 | −45.85829 | 2.8 | 0.5 | 53.7 | $4.2^{+2.6}_{-2.2}$ | $-1.00^{+0.36}$ | 1.2 | | |
| 164703.8-455349 | 251.76595 | −45.89698 | 2.8 | 0.5 | 53.7 | $6.8^{+2.3}_{-3.2}$ | $-0.62^{+0.37}_{-0.33}$ | 3.8 | | |
| 164650.8-454917 | 251.71167 | −45.82143 | 2.8 | 0.5 | 53.7 | $12.0^{+4.1}_{-3.4}$ | $-0.39^{+0.30}_{-0.30}$ | 5.1 | | |
| 164701.0-455350 | 251.75453 | −45.89733 | 2.9 | 0.5 | 53.7 | $7.6^{+2.9}_{-3.3}$ | $0.42^{+0.37}_{-0.40}$ | 5.3 | | |
| 164700.0-455349 | 251.75008 | −45.89697 | 2.9 | 0.5 | 53.7 | $8.6^{+3.2}_{-3.7}$ | $1.00_{-0.47}$ | 4.9 | | |
| 164720.1-455138 | 251.83397 | −45.86067 | 2.9 | 0.5 | 53.7 | $119.2^{+11.5}_{-11.2}$ | $1.00_{-0.03}$ | 100.0 | | 1 |
| 164720.3-455019 | 251.83496 | −45.83882 | 3.0 | 0.5 | 53.7 | $5.2^{+2.5}_{-2.2}$ | $-0.42^{+0.46}_{-0.43}$ | 2.7 | | 1 |
| 164715.0-454843 | 251.81268 | −45.81221 | 3.0 | 0.5 | 53.7 | $12.5^{+3.8}_{-4.1}$ | $0.46^{+0.26}_{-0.29}$ | 8.9 | | |
| 164653.4-454833 | 251.72290 | −45.80917 | 3.0 | 0.5 | 53.7 | $10.7^{+3.3}_{-3.9}$ | $-0.73^{+0.28}_{-0.25}$ | 4.1 | | 1 |
| 164721.2-455139 | 251.83861 | −45.86096 | 3.1 | 0.5 | 53.7 | $13.2^{+4.0}_{-3.8}$ | $0.78^{+0.17}_{-0.22}$ | 9.0 | | |
| 164716.6-454846 | 251.81938 | −45.81300 | 3.2 | 0.5 | 53.7 | $6.9^{+2.3}_{-3.3}$ | $-0.35^{+0.41}_{-0.40}$ | 4.0 | | 3 |
| 164721.3-455001 | 251.83900 | −45.83363 | 3.2 | 0.5 | 53.7 | $13.0^{+3.1}_{-4.4}$ | $-1.00^{+0.27}$ | 5.5 | | 1 |
| 164720.9-454940 | 251.83714 | −45.82781 | 3.3 | 0.5 | 53.7 | $9.0^{+3.5}_{-2.8}$ | $-1.00^{+0.35}$ | 3.8 | | 1 |
| 164646.1-455221 | 251.69250 | −45.87250 | 3.3 | 0.5 | 53.7 | $12.5^{+3.7}_{-4.1}$ | $-1.00^{+0.31}$ | 5.3 | | |
| 164648.8-455307 | 251.70352 | −45.88538 | 3.3 | 0.5 | 53.7 | $23.0^{+5.5}_{-4.9}$ | $-0.56^{+0.20}_{-0.19}$ | 12.4 | | 3 |
| 164643.8-455132 | 251.68289 | −45.85897 | 3.5 | 0.5 | 53.7 | $15.7^{+3.9}_{-4.5}$ | $0.15^{+0.25}_{-0.26}$ | 11.4 | s | |
| 164643.7-455128 | 251.68250 | −45.85786 | 3.5 | 0.5 | 53.7 | $2.9^{+1.3}_{-2.4}$ | $-1.00^{+0.47}$ | 1.0 | | |
| 164714.1-454800 | 251.80908 | −45.80006 | 3.5 | 0.5 | 53.7 | $16.9^{+3.8}_{-4.8}$ | $-0.85^{+0.18}_{-0.13}$ | 8.2 | | |
| 164652.6-455357 | 251.71956 | −45.89918 | 3.5 | 0.5 | 53.7 | $47.2^{+7.4}_{-7.1}$ | $-0.73^{+0.12}_{-0.10}$ | 24.3 | | |
| 164649.8-454824 | 251.70752 | −45.80682 | 3.5 | 0.5 | 53.7 | $16.8^{+4.4}_{-5.2}$ | $0.83^{+0.16}_{-0.19}$ | 13.0 | | |
| 164710.8-455420 | 251.79532 | −45.90556 | 3.6 | 0.5 | 53.7 | $7.4^{+3.1}_{-3.2}$ | $-1.00^{+0.65}$ | 3.1 | | 3 |
| 164720.3-454854 | 251.83496 | −45.81519 | 3.6 | 0.5 | 53.7 | $17.6^{+4.1}_{-4.7}$ | $-1.00^{+0.12}$ | 7.4 | | 13 |
| 164714.4-454754 | 251.81033 | −45.79861 | 3.6 | 0.5 | 53.7 | $7.7^{+2.7}_{-3.3}$ | $-0.18^{+0.39}_{-0.40}$ | 3.7 | | 1 |
| 164703.7-454723 | 251.76561 | −45.78982 | 3.6 | 0.5 | 53.7 | $12.3^{+3.9}_{-3.7}$ | $-1.00^{+0.37}$ | 6.2 | | |
| 164713.2-455413 | 251.80519 | −45.90369 | 3.6 | 0.5 | 53.7 | $27.8^{+5.1}_{-5.9}$ | $-0.47^{+0.18}_{-0.17}$ | 15.0 | 1 | 34 |
| 164725.8-455102 | 251.85780 | −45.85061 | 3.9 | 0.5 | 53.7 | $8.3^{+3.2}_{-3.1}$ | $1.00_{-0.40}$ | 5.3 | | |
| 164722.4-454851 | 251.84337 | −45.81437 | 3.9 | 0.5 | 53.7 | $3.7^{+1.8}_{-2.4}$ | $-1.00^{+0.39}$ | 1.3 | | |
| 164712.8-455435 | 251.80339 | −45.90976 | 3.9 | 0.5 | 53.7 | $17.6^{+4.2}_{-4.6}$ | $-0.53^{+0.23}_{-0.21}$ | 9.6 | | |
| 164717.9-455403 | 251.82484 | −45.90087 | 3.9 | 0.5 | 53.7 | $6.6^{+2.6}_{-3.0}$ | $-1.00^{+0.43}$ | 3.0 | s | 3 |
| 164641.4-455016 | 251.67288 | −45.83791 | 3.9 | 0.5 | 53.7 | $34.7^{+6.3}_{-7.0}$ | $0.40^{+0.17}_{-0.18}$ | 21.1 | 1 | |
| 164701.2-455457 | 251.75534 | −45.91600 | 4.0 | 0.5 | 53.7 | $11.2^{+4.2}_{-3.9}$ | $1.00_{-0.16}$ | 10.9 | | |
| 164718.7-454758 | 251.82797 | −45.79950 | 4.0 | 0.5 | 53.7 | $23.0^{+5.4}_{-4.8}$ | $-0.86^{+0.15}_{-0.12}$ | 11.9 | 1 | 134 |
| 164714.3-454725 | 251.80994 | −45.79041 | 4.0 | 0.5 | 53.7 | $7.7^{+2.9}_{-3.7}$ | $0.47^{+0.36}_{-0.40}$ | 4.2 | 1 | |
| 164640.0-455106 | 251.66705 | −45.85183 | 4.1 | 0.5 | 53.7 | $8.2^{+3.6}_{-3.4}$ | $-1.00^{+0.55}$ | 4.9 | | |
| 164641.0-455209 | 251.67087 | −45.86940 | 4.1 | 0.5 | 53.7 | $21.4^{+5.3}_{-5.3}$ | $0.26^{+0.23}_{-0.24}$ | 13.5 | 1 | |
| 164726.8-454959 | 251.86198 | −45.83310 | 4.2 | 0.5 | 53.7 | $8.1^{+3.4}_{-2.9}$ | $-1.00^{+0.48}$ | 4.3 | | |
| 164644.9-455335 | 251.68729 | −45.89329 | 4.2 | 0.5 | 18.8 | $9.0^{+2.7}_{-3.9}$ | $1.00_{-0.21}$ | 27.9 | | |
| 164713.0-454705 | 251.80428 | −45.78480 | 4.2 | 0.5 | 53.7 | $18.0^{+3.9}_{-5.2}$ | $-0.69^{+0.21}_{-0.18}$ | 10.0 | | 3 |
| 164728.0-455110 | 251.86682 | −45.85289 | 4.2 | 0.5 | 53.7 | $9.1^{+3.4}_{-2.9}$ | $-0.70^{+0.30}_{-0.25}$ | 4.7 | s | |
| 164716.2-454721 | 251.81769 | −45.78932 | 4.2 | 0.5 | 53.7 | $8.9^{+2.9}_{-4.0}$ | $0.50^{+0.32}_{-0.36}$ | 8.3 | | |
| 164700.2-454640 | 251.75124 | −45.77788 | 4.4 | 0.5 | 53.7 | $17.9^{+4.4}_{-5.6}$ | $1.00_{-0.30}$ | 15.9 | | |
| 164650.9-454708 | 251.71233 | −45.78566 | 4.5 | 0.5 | 34.9 | $11.9^{+3.4}_{-4.5}$ | $-0.03^{+0.32}_{-0.34}$ | 11.3 | | |
| 164659.8-455525 | 251.74954 | −45.92369 | 4.5 | 0.5 | 18.8 | $11.3^{+3.7}_{-3.6}$ | $0.57^{+0.25}_{-0.29}$ | 19.7 | | 34 |
| 164650.5-454700 | 251.71048 | −45.78359 | 4.6 | 0.5 | 34.9 | $6.7^{+2.8}_{-3.5}$ | $-1.00^{+0.32}$ | 3.2 | | |

**Table 1.** continued.

| X-ray Identifier | Right Ascension | Declination | Offset (arcmin) | Uncertainty (arcsec) | Detector Live Time (ks) | Net Counts | Hardness Ratio | Flux ($10^{-7}$ ph cm$^{-2}$ s$^{-1}$) | Variable? | C'part |
|---|---|---|---|---|---|---|---|---|---|---|
| 164640.8-454834 | 251.67041 | -45.80958 | 4.7 | 0.5 | 53.7 | $20.1^{+5.8}_{-5.4}$ | $0.83^{+0.17}_{-0.19}$ | 15.0 | 1 | |
| 164657.0-454627 | 251.73779 | -45.77442 | 4.7 | 0.5 | 34.9 | $10.0^{+3.0}_{-4.2}$ | $-0.36^{+0.35}_{-0.36}$ | 9.0 | | |
| 164728.9-454906 | 251.87062 | -45.81844 | 4.8 | 0.5 | 53.7 | $9.9^{+2.7}_{-3.9}$ | $-1.00^{+0.19}$ | 5.8 | | |
| 164730.3-454938 | 251.87653 | -45.82734 | 4.8 | 0.5 | 53.7 | $2.4^{+1.8}_{-1.9}$ | $-1.00^{+0.50}$ | 0.9 | | |
| 164635.6-455155 | 251.64871 | -45.86539 | 5.0 | 0.5 | 53.7 | $26.3^{+6.2}_{-6.0}$ | $-1.00^{+0.31}$ | 11.4 | | |
| 164640.0-454813 | 251.66678 | -45.80374 | 5.0 | 0.5 | 53.7 | $29.1^{+6.6}_{-6.0}$ | $1.00_{-0.15}$ | 30.1 | | |
| 164730.5-454914 | 251.87724 | -45.82061 | 5.0 | 0.5 | 53.7 | $5.5^{+2.4}_{-2.7}$ | $-0.33^{+0.47}_{-0.49}$ | 3.2 | | |
| 164648.6-454640 | 251.70273 | -45.77803 | 5.1 | 1.4 | 34.9 | $9.0^{+4.2}_{-3.6}$ | $-1.00^{+0.64}$ | 5.7 | | |
| 164719.7-455529 | 251.83231 | -45.92500 | 5.3 | 2.0 | 34.9 | $6.5^{+2.6}_{-2.9}$ | $0.21^{+0.41}_{-0.45}$ | 8.8 | | 3 |
| 164734.4-454943 | 251.89355 | -45.82883 | 5.5 | 1.3 | 53.7 | $14.4^{+4.3}_{-4.3}$ | $1.00_{-0.21}$ | 11.6 | | |
| 164647.1-454618 | 251.69656 | -45.77177 | 5.5 | 0.9 | 34.9 | $26.5^{+5.9}_{-6.2}$ | $1.00_{-0.16}$ | 39.3 | | |
| 164650.4-455600 | 251.71013 | -45.93354 | 5.5 | 1.4 | 18.8 | $11.6^{+3.6}_{-4.2}$ | $-1.00^{+0.22}$ | 15.6 | | 3 |
| 164731.7-455336 | 251.88228 | -45.89345 | 5.5 | 1.9 | 34.9 | $7.6^{+2.7}_{-3.2}$ | $-1.00^{+0.58}$ | 6.2 | | 3 |
| 164735.5-455113 | 251.89798 | -45.85374 | 5.5 | 2.7 | 53.7 | $2.3^{+2.0}_{-2.0}$ | $1.00_{-0.98}$ | 2.1 | | |
| 164636.2-454751 | 251.65117 | -45.79762 | 5.7 | 0.7 | 34.9 | $57.1^{+8.6}_{-8.0}$ | $-1.00^{+0.10}$ | 36.4 | | 34 |
| 164724.7-454622 | 251.85292 | -45.77303 | 5.9 | 3.0 | 18.8 | $5.2^{+2.6}_{-2.2}$ | $-1.00^{+0.57}$ | 8.3 | | |
| 164728.3-455505 | 251.86815 | -45.91825 | 5.9 | 1.5 | 34.9 | $14.2^{+4.4}_{-4.0}$ | $1.00_{-0.24}$ | 22.8 | | |
| 164737.1-454920 | 251.90482 | -45.82245 | 6.1 | 1.8 | 53.7 | $11.3^{+3.7}_{-3.5}$ | $-1.00^{+0.27}$ | 10.6 | | |
| 164723.5-455605 | 251.84802 | -45.93473 | 6.1 | 0.9 | 34.9 | $38.1^{+6.8}_{-6.3}$ | $-0.81^{+0.13}_{-0.11}$ | 31.9 | | |
| 164736.0-454744 | 251.90004 | -45.79568 | 6.5 | 2.2 | 18.8 | $9.9^{+2.8}_{-3.9}$ | $1.00_{-0.20}$ | 23.5 | | |
| 164655.6-454428 | 251.73203 | -45.74114 | 6.7 | 4.2 | 34.9 | $2.1^{+2.3}_{-1.9}$ | $1.00_{-0.49}$ | 18.2 | | |
| 164735.8-454656 | 251.89920 | -45.78223 | 6.9 | 3.8 | 18.8 | $6.2^{+2.9}_{-2.6}$ | $-1.00^{+0.40}$ | 8.3 | | |
| 164743.6-455214 | 251.93181 | -45.87071 | 7.1 | 2.3 | 53.7 | $12.6^{+4.0}_{-4.4}$ | $-0.44^{+0.31}_{-0.34}$ | 9.9 | | |
| 164629.4-455518 | 251.62253 | -45.92183 | 7.4 | 1.5 | 34.9 | $28.4^{+6.3}_{-6.4}$ | $0.57^{+0.18}_{-0.19}$ | 32.3 | | |
| 164631.3-455546 | 251.63075 | -45.92972 | 7.4 | 2.8 | 34.9 | $10.8^{+4.2}_{-5.1}$ | $-0.02^{+0.40}_{-0.48}$ | 13.4 | | 3 |
| 164655.2-455848 | 251.73016 | -45.98027 | 8.0 | 3.7 | 34.9 | $9.9^{+3.7}_{-4.7}$ | $0.21^{+0.40}_{-0.43}$ | 13.3 | | |
| 164748.4-454905 | 251.95195 | -45.81807 | 8.0 | 5.3 | 18.8 | $6.7^{+2.7}_{-3.3}$ | $-0.30^{+0.44}_{-0.47}$ | 10.5 | | |
| 164749.1-454930 | 251.95486 | -45.82524 | 8.1 | 7.1 | 18.8 | $2.1^{+2.0}_{-1.6}$ | $-1.00^{+0.80}$ | 4.3 | | |
| 164744.9-455459 | 251.93723 | -45.91652 | 8.2 | 3.5 | 34.9 | $11.6^{+4.0}_{-4.4}$ | $-1.00^{+0.40}$ | 12.1 | | 34 |
| 164633.9-455732 | 251.64142 | -45.95913 | 8.3 | 1.9 | 34.9 | $27.7^{+6.4}_{-7.1}$ | $0.60^{+0.19}_{-0.20}$ | 44.9 | | |
| 164745.4-454649 | 251.93919 | -45.78040 | 8.4 | 3.0 | 18.8 | $15.0^{+4.8}_{-4.1}$ | $0.78^{+0.18}_{-0.22}$ | 35.5 | | |
| 164700.2-455921 | 251.75124 | -45.98941 | 8.4 | 2.3 | 53.7 | $21.1^{+6.0}_{-5.4}$ | $-1.00^{+0.36}$ | 17.1 | | |
| 164732.2-455800 | 251.88438 | -45.96686 | 8.6 | 1.6 | 53.7 | $41.5^{+7.6}_{-7.8}$ | $-0.85^{+0.14}_{-0.13}$ | 30.1 | | |
| 164626.6-455642 | 251.61118 | -45.94506 | 8.6 | 4.4 | 34.9 | $10.3^{+5.4}_{-5.4}$ | $-1.00^{+0.40}$ | 7.7 | | |
| 164700.5-455937 | 251.75226 | -45.99373 | 8.6 | 2.2 | 53.7 | $26.1^{+6.9}_{-6.5}$ | $-0.16^{+0.25}_{-0.27}$ | 22.7 | | |
| 164737.4-455744 | 251.90622 | -45.96233 | 8.9 | 1.7 | 53.7 | $44.6^{+7.7}_{-8.1}$ | $-1.00^{+0.22}$ | 28.8 | | 3 |
| 164642.8-455920 | 251.67848 | -45.98901 | 9.1 | 2.1 | 34.9 | $32.7^{+7.0}_{-7.7}$ | $-0.67^{+0.20}_{-0.22}$ | 36.3 | | 3 |
| 164750.5-455540 | 251.96069 | -45.92794 | 9.4 | 3.1 | 53.7 | $20.7^{+6.3}_{-6.9}$ | $-1.00^{+0.18}$ | 9.9 | | |
| 164753.4-454651 | 251.97253 | -45.78088 | 9.6 | 4.3 | 18.8 | $14.8^{+4.4}_{-5.3}$ | $-1.00^{+0.25}$ | 24.9 | | 3 |
| 164610.4-455448 | 251.54375 | -45.91344 | 10.0 | 2.8 | 34.9 | $30.2^{+7.8}_{-7.4}$ | $-0.44^{+0.24}_{-0.28}$ | 39.0 | | |
| 164730.3-455954 | 251.87627 | -45.99844 | 10.0 | 4.8 | 18.8 | $15.3^{+5.2}_{-5.0}$ | $-0.47^{+0.31}_{-0.34}$ | 31.5 | | |
| 164650.7-460058 | 251.71127 | -46.01613 | 10.2 | 2.7 | 53.7 | $34.4^{+8.8}_{-8.8}$ | $-0.23^{+0.24}_{-0.28}$ | 27.9 | | 3 |
| 164748.2-454409 | 251.95110 | -45.73602 | 10.4 | 4.7 | 18.8 | $17.1^{+5.5}_{-5.1}$ | $-0.55^{+0.28}_{-0.31}$ | 35.5 | | 34 |
| 164746.0-455904 | 251.94176 | -45.98446 | 10.9 | 1.7 | 53.7 | $108.3^{+12.5}_{-12.4}$ | $0.58^{+0.09}_{-0.09}$ | 90.0 | | 3 |
| 164623.7-455928 | 251.59908 | -45.99132 | 11.0 | 5.6 | 34.9 | $17.2^{+6.5}_{-6.1}$ | $-1.00^{+0.27}$ | 15.5 | | |
| 164658.6-460237 | 251.74451 | -46.04364 | 11.7 | 10.0 | 53.7 | $10.1^{+6.5}_{-6.1}$ | $-1.00^{+0.30}$ | 4.0 | | |
| 164805.7-455643 | 252.02393 | -45.94548 | 12.2 | 2.7 | 18.8 | $70.1^{+9.7}_{-9.3}$ | $-0.88^{+0.09}_{-0.09}$ | 155.1 | | |
| 164759.8-455901 | 251.99921 | -45.98367 | 12.6 | 3.3 | 18.8 | $58.3^{+9.0}_{-8.8}$ | $-0.78^{+0.12}_{-0.12}$ | 105.4 | | |
| 164555.5-455600 | 251.48155 | -45.93354 | 12.9 | 3.5 | 34.9 | $57.6^{+10.0}_{-10.4}$ | $-0.21^{+0.17}_{-0.19}$ | 102.2 | | 34 |
| 164629.0-460229 | 251.62114 | -46.04152 | 13.0 | 6.1 | 34.9 | $28.1^{+7.5}_{-7.0}$ | $0.36^{+0.22}_{-0.23}$ | 28.1 | | |
| 164700.1-460559 | 251.75063 | -46.10000 | 15.0 | 8.0 | 53.7 | $35.1^{+9.3}_{-8.7}$ | $0.01^{+0.25}_{-0.26}$ | 35.2 | | |
| 164658.2-460639 | 251.74281 | -46.11097 | 15.7 | 10.0 | 34.9 | $30.4^{+8.2}_{-8.3}$ | $0.63^{+0.23}_{-0.22}$ | 67.2 | | |
| 164702.5-460701 | 251.76062 | -46.11713 | 16.0 | 10.0 | 53.7 | $20.8^{+6.6}_{-7.5}$ | $-0.58^{+0.29}_{-0.35}$ | 29.2 | sl | |
| 164704.1-460710 | 251.76743 | -46.11953 | 16.2 | 10.0 | 53.7 | $17.7^{+6.4}_{-7.1}$ | $-1.00^{+0.49}$ | 15.8 | sl | |
| 164653.3-460722 | 251.72249 | -46.12304 | 16.5 | 5.4 | 34.9 | $88.5^{+11.4}_{-11.8}$ | $-0.45^{+0.12}_{-0.12}$ | 108.6 | | 3 |
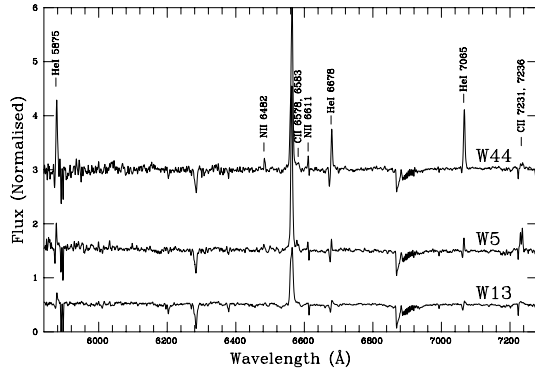
**Fig. A.1.** Plot of the *R* band spectrum of the WNVLs W44 and W5 and the BIa$^+$ star W13, showing the continuity in spectral properties of the three stars.

## Appendix A: Spectral classifiction of X-ray counterparts

### A.1. Classical Wolf-Rayet stars

Crowther et al. (2006) utilise near-IR spectroscopy to classify all 24 WRs within Wd 1, resulting in a re-classification of 8 of the 12 X-ray bright WRs (Table 3). Of these, only the WN7b star WR A exhibits spectroscopic signatures of binarity, with absorption features superimposed on both the broad He I 1.083 and 2.0589 $\mu$m emission lines suggestive of an early super-giant companion. The WR component of a putative OB+WR binary is expected to dominate emission at near-IR wavelengths (Crowther et al. 2006); thus we do not expect any further WRs to be present but undetected within the population of X-ray bright OB SGs unless they are significantly underluminous compared to those currently identified. Unfortunately, traditional classification criteria for putative O (e.g He II absorption) or B star (He I) companions lie in the 4000−5000 Å region which is inaccessible due to high interstellar reddening and so we may not offer more than a generic WR+luminous OB companion classification for potential WR binary systems (Sect. 4.1). We see no spectroscopic evidence for any WR+WR binaries.

### A.2. Transitional late Wolf-Rayet stars and B super/hypergiants

In Fig. A.1 we present the *R* band spectra of W44 (=WR L; WN9h) and W5 (=WR S; formally WN10-11h or BIa$^+$) and W13 to demonstrate the close continuity in physical properties between the three stars. All show strong H$\alpha$ emission, which decreases in strength from W44 through W5 to W13, a trend also seen in the He I lines, while C II is observed in emission in W5 but is in absorption for W13. Consequently, we suggest that W13 has a weaker wind than W44 or W5 and propose an early BIa$^+$ classification to be most appropriate. No spectroscopic evidence for binarity is seen for any of these three objects.

On the basis of its high luminosity, rich emission spectrum and IR excess, W9 has previously been classified as a post-MS (supergiant) sgB[e] star, albeit with the anomalous presence of [O IV] emission in an ISO spectrum of the source (Clark et al. 1998). Formally, Lamers et al. (1998) require the presence of [O I] and [Fe II] emission lines in the optical spectrum for a sgB[e] classification; however prior data were of insufficient S/N and spectral range to verify their presence. Our new high S/N spectra allow us to identify these features for the first time (Fig. A.2). Emission from a large number of additional species
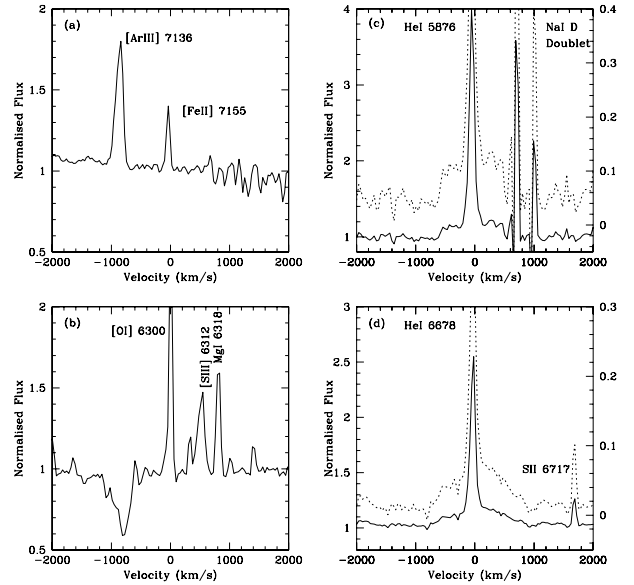


**Fig. A.2.** Plots of selected regions of the ∼5500−7500 Å spectrum of the candidate sgB[e] star W9. Panels **a)** and **b)** present the regions centred on the [O I] 6300 Å and [Fe II] 6300 Å forbidden line transitions and also include transitions from the previously undetected species Mg I, S III and Ar III. Panels **c)** and **d)** present the He I 6876 Å and 6678 Å transitions, illustrating the broad emission plinths present; we also over-plot the log of the normalised fluxes (dotted lines – scale on right axis) in order to emphasise these features.

is observed[19] – although no high excitation species such as He II appear to be present despite the [O IV] emission.

The H$\alpha$ line profile of W9 broadly mirrors those of other B[e] stars (Zickgraf 2003), with a narrow central peak (*FWHM* ∼ 250 km s$^{-1}$) and broad emission wings (>1400 km s$^{-1}$; due to electron scattering). Likewise, low excitation permitted and forbidden metallic emission lines are narrower (e.g. *FWHM* ∼ 80 km s$^{-1}$ for [O I] 6300 Å), with Zickgraf et al. (2003) attributing the different line profiles to an anisotropic wind with a dense, slow equatorial outflow and a higher velocity polar wind. However close examination of the He I 5876 and 6678 Å (Fig. A.2) profiles reveals a narrow emission core superimposed on a broad emission plinth extending to large projected velocities (∼−600/+500 km s$^{-1}$ and ∼−800/+900 km s$^{-1}$ respectively), implying a high velocity outflow. Such profiles are unknown for any other B[e] star (Zickgraf 2003), and, to the best of our knowledge for any other massive mass losing star, with the possible exception of the composite nebular+stellar spectra of $\eta$ Carinae (cf. the He I 7065 Å profile presented in Smith et al. 2003).

### A.3. The OB supergiants

In total >70 O9-B4Ia/b supergiants have been spectroscopically identified within Wd 1 (Clark et al. 2005, Negueruela et al. in prep.). Due to the high interstellar reddening towards Wd 1, traditional blue end classification criteria for OB supergiants are unavailable to us and hence we are forced to rely on *R* and *I* band observations. A full description of this process will be presented in Negueruela et al. (in prep.); here we limit ourselves to presenting the new high resolution and S/N *R* band spectra of 10 X-ray bright OB supergiants (Fig. A.3). The spectrum of W40a may

---

[19] H I, He I, O I, N II, Fe II, Ca II, Mg II, Ni III, S II, S III and Ar III.
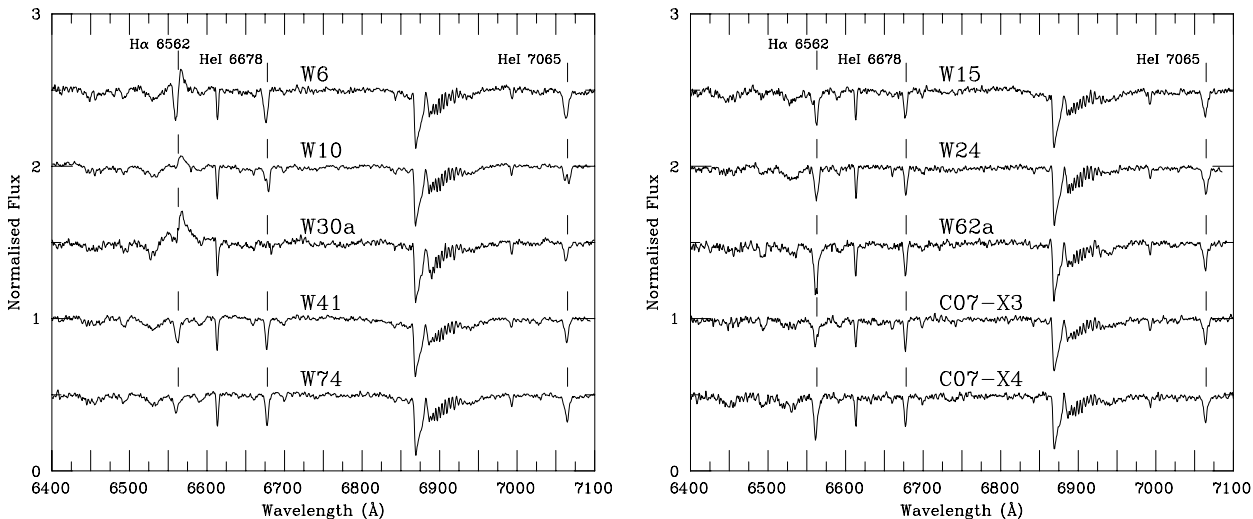
**Fig. A.3.** *R* band spectra of 10 candidate O9-B0 Ia supergiants with associated X-ray emission.

be found in Clark et al. 2005), while the low S/N NTT/EMMI spectra of W25 and W27, while discussed below are omitted for brevity and will be presented in Negueruela et al. (in prep.).

In spite of the scarcity of features in the *R* band spectra of OB stars, several can be used for classification purposes (an *I* band classification scheme is given in Appendix A of Clark et al. 2005). Unfortunately, most of these are sensitive to both spectral type and luminosity, but by using several of them at the same time, we can generally narrow the spectral range for a given star down to half a spectral type. Of these criteria we employ: the shape and strength of H$\alpha$ (P Cygni emission), the C II 6578,6582 Å (in absorption) and C II 7231, 7236 Å (in emission) doublets, the O I 7774 Å triplet (in absorption) and the N II 6482 Å (absorption) line.

Seven of the ten OB stars demonstrate remarkably similar spectra, characterised by (i) H$\alpha$ and He I 6678 and 7065 Å in absorption, (ii) a lack of photospheric C II 6578 and 6582 Å and O I 7774 Å absorption and (iii) no Si IV 6669 and 6701 Å emission. The latter observation constrains the spectral types to ~O9I or latter, while the lack of photospheric C II (O I) absorption restricts it to ~B0I (B0.5I) or earlier. The H$\alpha$ and He I absorption features are also consistent with such an interpretation; W62a and C07-X3, for which the photospheric H$\alpha$ profile is stronger than the He I transitions, are likely of a lower luminosity, which results in less wind emission. Thus we classify these stars in the range O9-9.5Ia, with the two aforementioned stars possibly of luminosity class Iab or Ib.

The presence of strong, broad H$\alpha$ emission profiles is suggestive, *but not conclusive* of a binary nature for W6, 10 and 30a. Excess H$\alpha$ emission is seen in binaries composed of both OB+OB (Thaller 1997) and OB+compact object binaries (Negueruela et al. 2005); hence we are unable to determine the nature of the companions to W6 & W30a from these data alone. However, the presence of broad, double "troughed" He I 6678 and 7065 Å profiles in W10 clearly indicates a luminous OB companion. Rapid night to night variability is observed in the H$\alpha$ profile of W30a (Fig. A.4) – again a strong indicator of binarity (e.g. Negueruela et al. 2005). Unfortunately, the presence of the emission contaminates both the intrinsic H$\alpha$ and C II 6578 and 6582 Å profiles and so we are forced to limit ourselves to an O9-B0.5Ia classification for these systems.
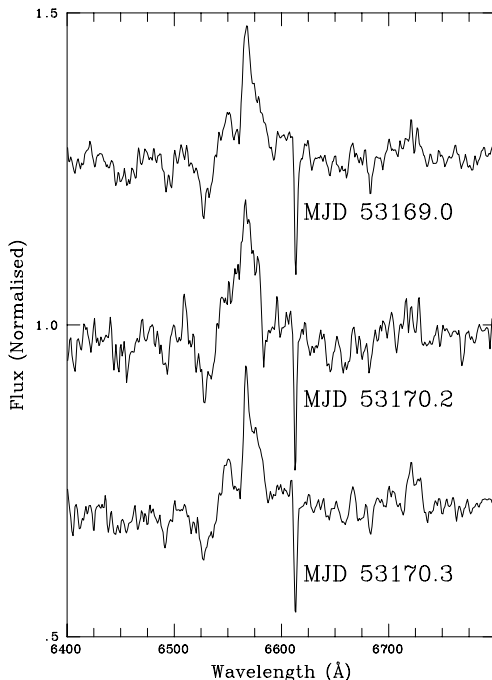


**Fig. A.4.** Plot of the H$\alpha$ profile of W30a on 2004 June 12–13 demonstrating short term variability indicative of an interacting binary.

Finally, spectral classification of W25 and W27 is complicated by the low S/N of the spectra. Based on the above criteria , both stars appear to be OB supergiants, with the presence of strong, possibly variable H$\alpha$ emission hinting at binarity for W27.

### A.3.1. Classification from photometric data

Unfortunately, a large number of optical counterparts lack spectroscopy and so we are forced to rely on photometric classification calibrated by the optical spectroscopy of Negueruela et al. (in prep.). In the main panel of Fig. A.5 we present a colour magnitude plot for the cluster members, indicating both those stars for which spectral classifications exist, as well as those which have an X-ray detection.
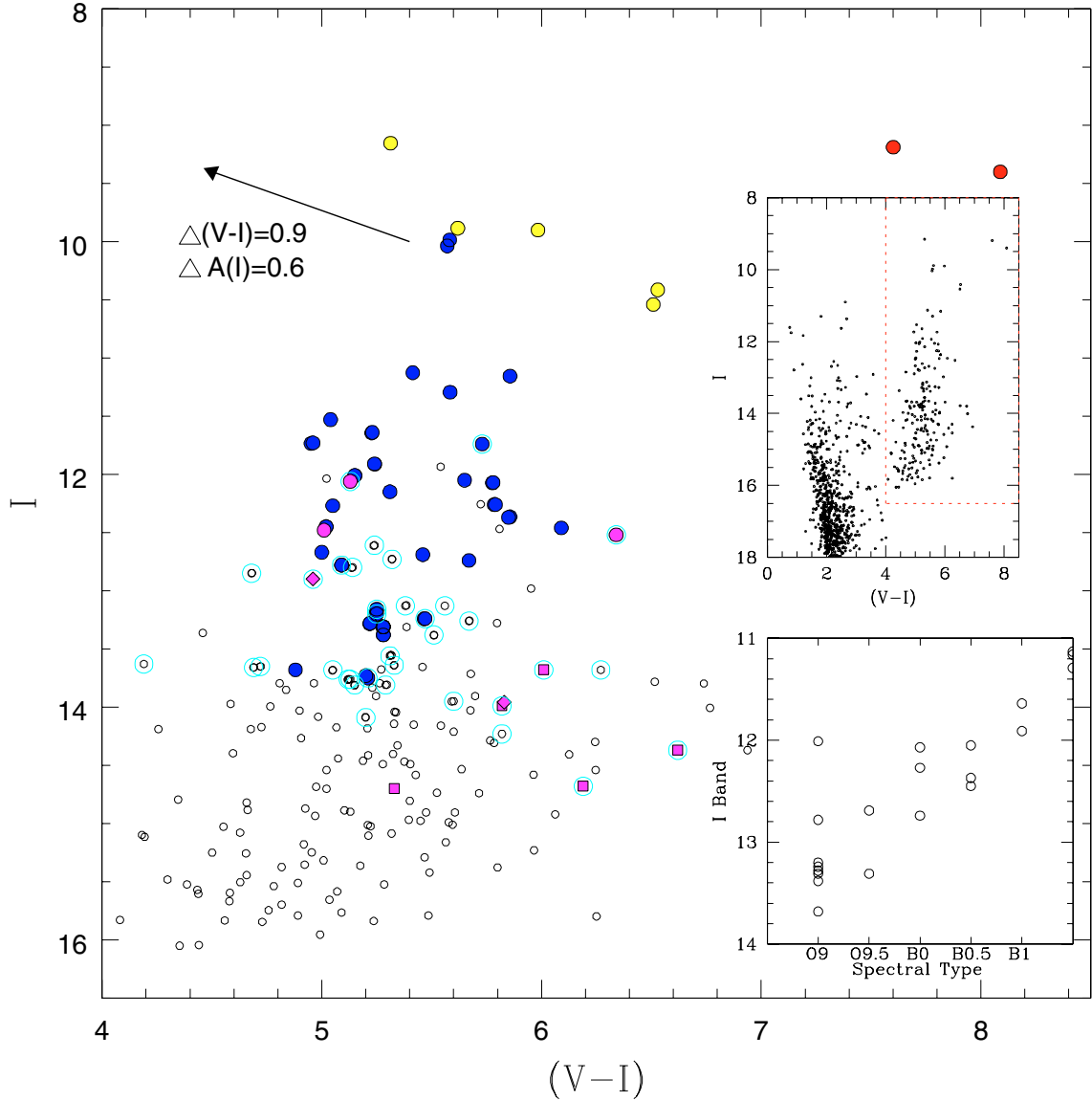
**Fig. A.5.** *Main panel*: $(V-I)/I$ band colour magnitude plot for the central $5' \times 5'$ field enclosing Wd 1, subject to a colour cut in order to emphasise cluster members (*panel* **a**) shows the full dataset of Clark et al. 2005). Stars associated with X-ray sources are circled. Filled symbols correspond to those stars with spectral classifications: red – RSGs, yellow – YHGs, blue – BSGs and magenta – the WNLs & WNL/BIa$^+$ hybrid (circles), WNs (squares) and WCs (diamonds). The effect of differential reddening across the cluster is indicated by the vector. *Panel* **b**): plot of $I$ band magnitude versus spectral type for OB supergiants with spectral classifications. We caution that not all the stars for which spectra are available are present due to blending (supergiants and hypergiants) or faintness (WRs).

For stars of $35-40\,M_\odot$ post-MS evolutionary tracks traverse the HR diagram at ~constant luminosity, while bolometric corrections decrease from $-2.97$ to $-1.83$ for O9-B1.5 Ia stars respectively; hence at optical wavelengths one would expect stars with later spectral types to be systematically brighter than those with earlier spectral types. Comparison of the $I$ band magnitudes of the complete sample of stars with spectral classifications suggests that this is indeed the case (Fig. A.5, panel b)[20].

Excluding the sgB[e] star W9 ($I \sim 11.7$) the BIa$^+$ star W13 ($I \sim 12.1$) and the WR stars, the remainder of the optical counterparts to X-ray sources are found within a narrow range of $I$ band magnitudes, with none brighter than $I = 12.5$. We therefore classify these stars as B0.5Ia-O9Ia – the latter being the earliest spectral type observed for SGs within Wd 1 – consistent with the results of our spectroscopy.

---

[20] We note that there is a significant scatter in magnitudes for stars of apparently identical spectral type. Differential reddening likely causes a ~0.6 mag dispersion in the $I$ band, but clearly cannot account for the full range of magnitudes. Other effects which may contribute are: (i) unresolved binarity (ii) uncertainties in the spectral classification and hence bolometic correction and (iii) a genuine scatter in the intrinsic magnitudes of stars of the same spectral type, possibly due to variations in rotational velocity (e.g. Meynet & Maeder 2003); a full account of these effects is beyond the scope of this paper.